Experimental study of battery passive thermal management system using copper foam-based phase change materials

Sun, Z., Guo, Y., Zhang, C., Whitehouse, J., Zhou, Q., Xu, H. & Wang, C.

DOI 10.1016/j.ijft.2022.100255
ISSN 2666-2027

Publisher: Elsevier

17 (2023) 100255

Contents lists available at ScienceDirect

International Journal of Thermofluids

journal homepage: www.sciencedirect.com/journal/international-journal-of-thermofluids

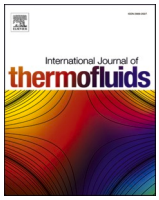

Experimental study of battery passive thermal management system using copper foam-based phase change materials

Zeyu Sun [a,b], Yue Guo [a], Cheng Zhang [a], Jon Whitehouse [c], Quan Zhou [b], Hongming Xu [b], Chongming Wang [a,*]

[a] Institutes for Future Transport and Cities, Coventry University, Coventry, CV1 5FB, United Kingdom
[b] Department of Mechanical Engineering, University of Birmingham, Birmingham, B15 2TT, United Kingdom
[c] Ecobat Solutions UK, Darlaston, WS10 8JR, United Kingdom

ARTICLE INFO

Keywords:
Lithium-ion battery
Composite phase change material
Thermal management
Thermal dummy cell

ABSTRACT

Lithium-ion batteries (LiBs) have been widely applied in electric vehicles (EVs) and energy storage devices. The battery thermal management system (BTMS) critically impacts the safety and degradation of LiBs. Phase change material (PCM) is a promising passive BTMS solution owing to its high latent heat and non-parasitic power consumption requirements. In this paper, paraffin (PA) as the PCM was embedded in the copper foam to enhance the heat dissipation of the cooling material. The thermal responses of the battery module were comparatively investigated under different thermal management solutions, including natural air, pure PCM, and copper foam-PCM. A battery module consisting of 16 thermal dummy cells (TDC) was designed, built, and calibrated to replace real commercial 21,700 NMC battery cells. The findings indicate that the proposed copper foam-PCM solution effectively enhances heat dissipation and improves the temperature uniformity of the battery module. For instance, in the condition of intensive operation (60% depth of discharge and 3C discharge), copper foam-PCM composite material reduces the maximum temperature rise from 57.4 °C to 51.4 °C (-10.4%) compared to pure PCM. At ambient temperatures of 25 °C and 35 °C, the temperature inhomogeneity of the battery module with copper foam-PCM is maintained within 5 °C and 2 °C, respectively. Besides, the effect of copper foam-PCM cooling on the cell-to-pack conversion efficiency was evaluated. The gravimetric cell-to-pack ratio (GCTP) and volumetric cell-to-pack ratio (VCTP) of the battery pack employing the proposed BTMS reached 53.1% and 45.6%, respectively.

1. Introduction

Nowadays, vehicle electrification technologies have been vigorously developed to reduce global greenhouse gas emissions [1]. Lithium-ion batteries (LiBs) with high specific power and high energy density are widely applied in the automobile industry as promising energy storage devices. The charging and discharging of LiBs are accompanied by heat generation, including ohmic heat, polarization heat, side reaction heat, and mixing heat. A battery thermal management system (BTMS) plays an important role in ensuring the performance, safety, and service life of LiBs [2]. The safe temperature for LiBs used in electrified vehicles is limited to 60 °C [3,4]. An excessively high temperature might lead to battery thermal runaway, fire, and even explosion [5]. BTMS is intended to maintain LiBs temperature within the optimal range from 15 °C to 35 °C, while the temperature non-uniformity of batteries in a module/pack is below 5 °C [6,7]. At present, thermal management methods have evolved from conventional air-based cooling [8] and indirect liquid-based cooling [9,10] to phase change material (PCM) cooling [11], heat pipe [12,13], and immersion cooling [14]. In active cooling systems, pumps or fans induce parasitic power consumption. Passive cooling systems, such as PCMs or heat pipes, don't consume extra energy while dissipating the surface temperature of batteries [15]. Jouhara et al. [16] proposed a BTMS consisting of heat pipes that eliminate approximately 60% of the heat generation of LiBs and significantly enhance temperature uniformity within the battery module.

Due to its high latent heat and non-parasitic power consumption, PCM is regarded as a promising passive BTMS solution. Chen et al. [17] proposed the BTMs with PCM. Simulation results evaluated that PCM led to high-temperature uniformity in the battery module. Paraffin (PA) was

* Corresponding author at: Institute for Clean Growth & Future Mobility, 1 Gulson Road, Coventry, CV1 2JH, United Kingdom
E-mail address: ac8174@coventry.ac.uk (C. Wang).

https://doi.org/10.1016/j.ijft.2022.100255

Available online 29 November 2022

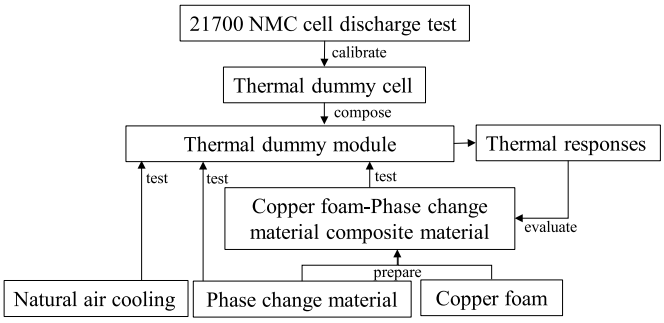

Fig. 1. Schematic diagram of the experimental study design.

Table 1
Specifications of 21,700 NMC811 battery cell [44].

Item	SSpecification
Nominal Voltage	3.7 V
Typical Capacity	4800mAh
Cathode	Graphite
Ano'de	NMC811
Internal resistance	0.035 Ω

applied as PCM for the BTM system due to its low cost and suitable phase change temperature [18]. However, the disadvantage of PA is its low thermal conductivity (0.2 W/m/K) [19]. To improve the performance of PCMs in heat dissipation, PCM was integrated with various materials with high thermal conductivity, such as expanded graphite (EG) [20], graphene [21], carbon nanofiber [22], and metal foams [23], to produce composite materials. Sheikh et al. [24] experimentally investigated the cooling performance of bio-based PCM with graphene nanoplatelets and surfactants. PA may sink due to gravity after the repeated melting-solidification process, resulting in an increased temperature gradient in the battery module. Metal foams with porous structures have a large surface area-to-volume ratio and enhance heat transfer [25]. Alrashdan et al. [26] examined the thermo-mechanical properties of PCM composite materials at different operating temperatures. Qu et al. [27] adopted the finite element method to investigate PCM-metal foam composite materials. The results show that the BTMS with PCM-metal foam composite phase change materials was more effective in reducing the battery surface temperature at the discharge rates of 1 C and 3 C compared to the air convection cooling method. Sheikh et al. [28] evaluated the effect of copper foam with different pore sizes on the Melting performance of PCM. Xiao et al. [29] explored the effect of impregnating the nickel foam and copper foam with PA under vacuum on their thermal performance. The results illustrated that reducing the metal foam porosity would improve thermal conductivity, despite no significant effect of foam pore size on the level of thermal conductivity. Chen et al. [17] applied a numerical model to investigate the thermal performance of the air-cooling and PCM cooling methods at various high current and ambient temperatures. A separate investigation was conducted into the effect of two cooling methods used for BTMs on the degradation and parasitic power consumption of batteries. Zhao et al. [30,31] experimental and numerical investigated the composite PCM as the heat sink on the cooling performance of a liquid cooling-based BTMS, and they established the relationships of the Nusselt numbers and dimensionless temperature against the Fourier and Stefan numbers. Sundarram et al. [32] conducted a numerical study as to the impact of the porosity and pore size on the thermal properties of a metal foam embedded with PCM. Wang et al. [33] explored the thermal conductivity of paraffin-aluminum foam composite PCM, demonstrating that the aluminum foam is capable to improve the thermal conductivity of PA. Despite the inhibitory effect of aluminum foam on local natural convection, it could accelerate the melting process and enhance the temperature uniformity of PCM. PA has high flammability properties. Li et al. [34] added melamine and triphenyl phosphate to PA, which improves the flammable retardant performance of composite material. Weng et al. [35] investigated the mitigation effects of PCM with the different proportions of flame retardant additive (Aluminum hydroxide) on thermal runaway propagation. Due to the conductivity of copper foam, conducting electricity between metal foam and LiBs should be considered in the design of the thermal management system, which prevents short circuits inside the battery module. Conventionally, PA is considered to be a non-conductive material. Wu et al. [36] proposed a BTMS mesh-enhanced composite. The sandwich structure of composite material effectively avoids direct contact between the metal material and the prismatic battery. Due to the simplicity and the buffer protecting effect of the battery module, the thermal management strategy with PCM composite material as a cooling medium has a potential for application in BTMS.

A large majority of the electric energy stored in the battery is consumed by the load, and only 2.89% to 7.89% of the electric energy is converted into heat at discharge rates of 1C to 2.5C, respectively [37]. The maximum acceptable constant current load of LiBs used in EVs is approximately 3C-rate [38,39]. Besides, the charging/discharging process of the battery is a time-consuming process, which extends the test period. Repeated heating tests of batteries can cause battery degradation, thereby increasing the heat generation rate. In addition, battery discharging under high-power conditions is restricted by capacity, which makes it difficult to conduct the battery test under extreme heating conditions. The potential safety hazard caused by the overheating of the battery and the high experimental cost incurred by safety-related equipment is also the main constraints on carrying out experiments with real batteries. To address the above problems, a thermal dummy cell (TDC) is used as a replacement for the real battery cells in the research of thermal management. Volck et al. [40] investigated the internal short-circuit resistance of a specially constructed dummy pouch battery cell under various compressive loads. The dummy battery cell was filled with a solvent without the conductive medium. The short-circuit resistance was analyzed mathematically following a short-circuit experiment on dummy batteries with an external power supply. Zhu et al. [41] applied a dummy thermal battery to evaluate the thermal performance of a pumped two-phase BTMS at the heat fluxes ranging from 0.11 W/cm^2 to 0.60 W/cm^2. Wang et al. [42] adopted a hybrid multi-cell pack (12 prismatic dummy cells and 4 real batteries) to develop an actively controlled BTMS. To investigate the effect of moist air on real battery operating, Saw et al. [43] developed a cylindrical TDC with a constant 5 W heating power.

As can be seen from the aforementioned studies, the experimental examination of copper foam-PCM cooling for battery modules is limited, especially at high ambient temperatures, which is essential for further revealing the heat dissipation performance of copper foam-PCM and its applications in the BTMS. Additionally, the impact of thermal management strategies on the cell-to-pack conversion efficiency has not yet been investigated. Herein, a passive cooling system with the PCM-copper foam composite material was built to improve the thermal performance of the battery module. The copper foam was selected as the porous material for the thermal conductivity enhancement of PCM. Thermal imaging technology and thermocouples were used to monitor the temperature evolution of the battery modules at the ambient temperature of 25 °C and 35 °C. On the other hand, the investigations of thermal characteristics of 21,700 NMC battery cells and feasibility study of TDC on BTMS design are still inadequate. A TDC was developed to substitute the real 21,700 NMC LiBs. By adjusting the power supply voltage, the aluminum alloy block integrated with a built-in heater can be used to mimic the heating power of the real batteries at various discharging constant current rates. The thermal behavior of TDC is validated against real 21,700 NMC battery cells.

The influence of the copper foam-PCM cooling method on the mass and volume of the battery pack was evaluated by cell-to-pack conversion

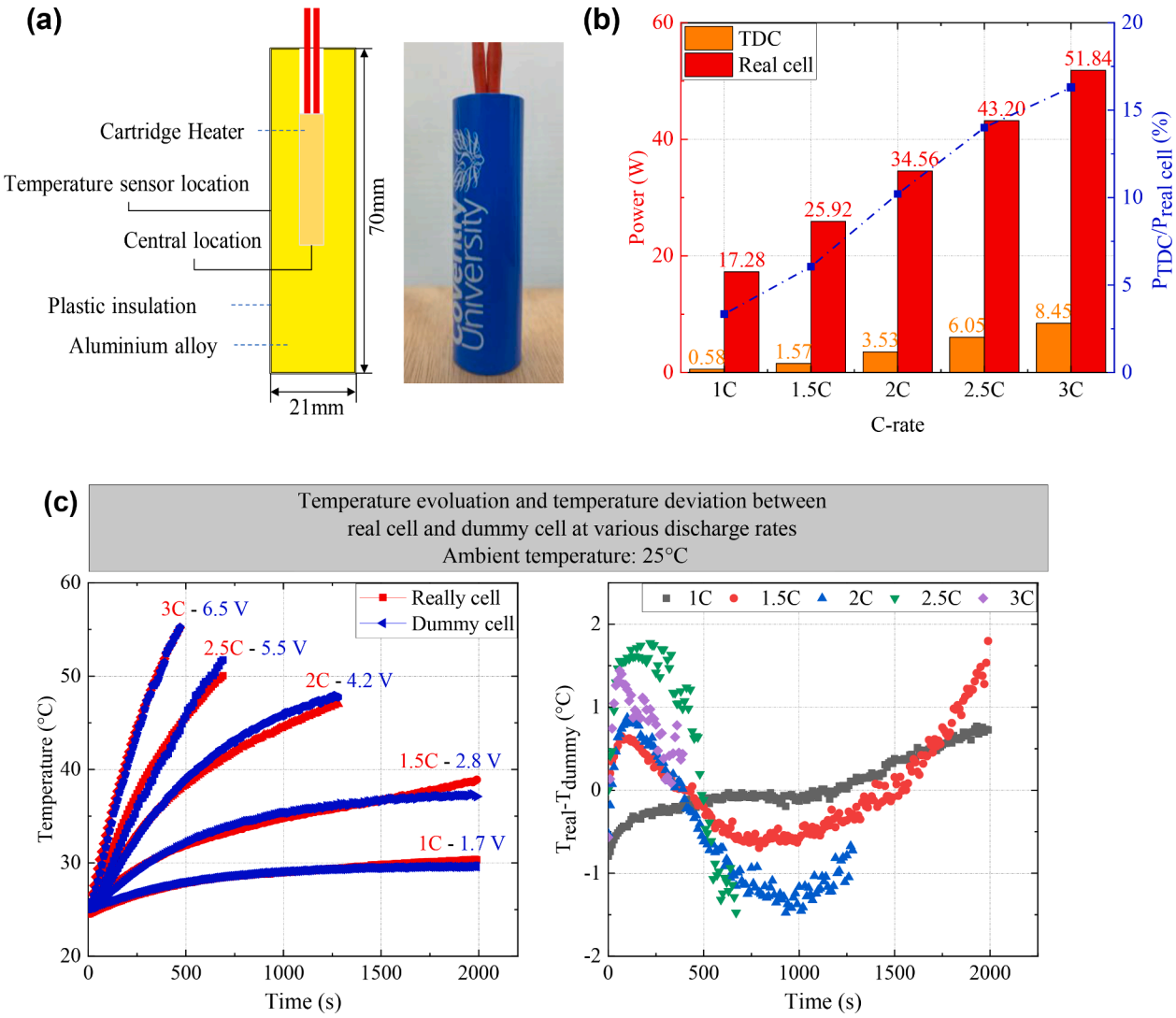

Fig. 2. The experimental setup for TDC: (a) Longitudinal section and practicality diagram of TDC; (b) Electrical power consumption of the TDC and real cell; (c) Temperature evolution of TDC and real cell at various discharge rates.

Table 2
Theoretical heat generation rate of real battery cell and the heat generation rate of TDC at various discharge rates.

C-rate	$q_{theoretical}$	q_{TDC}
1C	0.8 W	0.6 W
1.5C	1.8 W	1.6 W
2C	3.2 W	3.5 W
2.5C	5.0 W	6.0 W
3C	7.3 W	8.5 W

efficiency on a gravimetric (GCTP) and volumetric (VCTP). The rest of this paper is organized as follows: the experimental setup and test procedures are introduced in Section 2. The results and discussion are illustrated in Section 3. Finally, the conclusions of the main findings are presented in Section 4.

2. Experimental setup and procedures

This part is divided into three sub-sections, including the design of thermal dummy cells, preparation of the battery module with cooling material, and test procedures. A competitive study was performed, including natural air cooling, pure PCM cooling, and copper foam-PCM cooling. The detailed schematic diagram of the experimental study design is illustrated in Fig. 1.

2.1. Thermal dummy cell

The cylindrical dummy cells are utilized to replace the real LG 21,700 NMC811 batteries, the specifications of which are listed in Table 1. The reasons for the use of dummy cells instead of real battery cells are as follows: 1) No need to use expensive battery module cyclers; 2) TDCs could avoid the potential thermal/electrical hazards of battery modules operated under extreme conditions; 3) TDCs reduce energy consumption and test time; 4) TDCs can avoid results drift caused by battery degradation. Fig. 2.(a) depicts the TDC. An electric cartridge heater with an internal resistance of 5 Ω is inserted into a cylindrical aluminum alloy with a concentric hole (diameter: 6.5 mm; depth: 45 mm). The heat generation rate of cartridge heaters is controlled by the adjusting voltage. The calculation formula of heat generation can be described as:

$$q_{TDC} = U^2 / R_{TDC} \quad (1)$$

where R_{TDC} represents the resistance of the cartridge heater, and U represents the voltage.

A procedure was developed to conduct TDC voltage calibration for

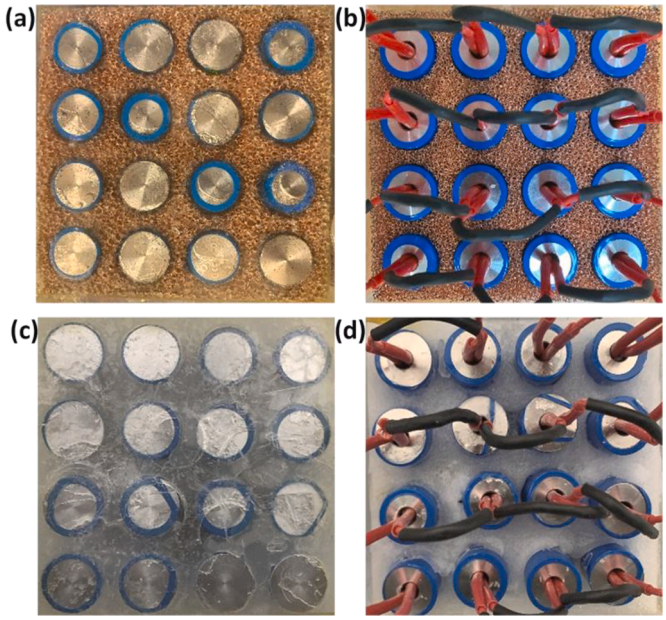

Fig. 3. Battery module with cooling material: (a) copper foam-PCM, bottom view; (b) copper foam-PCM, top view; (c) pure PCM, bottom view (d) pure PCM, top view.

Table 3
Thermophysical parameters of battery cell and materials.

Item	Battery [45]	Aluminum [46]	Copper [46]	PCM [47]	Air
Density (kg/m^3)	2616	2719	8978	900	1.2
Thermal conductivity (W/m/K)	1.3 (radial)/ 20.7 (axial)	202.4	386	0.2	0.02
Specific heat capacity (J/kg-K)	910	871	381	2220	1005
Latent heat (kJ/kg)	NA	NA	NA	137	NA
Melting temp. (°C)	NA	660	1085	40	NA

the purpose of matching the thermal behavior of TDC with real cells. The voltage applied to dummy cells was swept, and the surface temperature of dummy cells was monitored. Real cells were discharged under various C rates (1C - 3C), and surface temperature was measured. It is possible to find the best matching voltage required for dummy cells to simulate its thermal behavior for a real battery discharged at a certain discharge rate. It is found that the temperature evolution of the dummy cell under the voltage of 1.7 V, 2.8 V, 4.2 V, 5.5 V, and 6.5 V matched well with that of the real cell under discharging rates of 1C, 1.5C, 2C, 2.5C, and 3C, respectively. Fig. 2(b) shows the electrical power consumption of the TDC and a real cell in the experiment. Fig. 2(c) illustrates the comparison of temperature evolution between TDC and real cells. It can be seen that with a proper TDC voltage calibration, the surface temperatures of dummy and real cells match well under various constant discharge rates. Some literature calculates the theoretical heat generation rate of battery cells based on Ohm's law [3,14]:

$$q_{real} = I^2 R_0 \tag{2}$$

where R_0 represents the internal resistance of the real battery cell, and I represents the discharging current.

Table 2 lists the theoretical heat generation rate of the battery and the heat power of TDC under various constant discharge rates. The reasons for the difference between the theoretical heat generation rate of the battery cell and the heat power of TDC are 1) Eq. (2) only considers irreversible heat, which ignores reaction to heat and side reaction heat during battery operation; 2) In terms of heat transfer characteristics, battery cell can be regarded as anisotropic, and the radial thermal conductivity is lower than the axial thermal conductivity. TDC made by aluminum alloy are isotropic heat transfer and its radial/axial thermal conductivity is also significantly higher than that of the real cell. Therefore, the verification of the heating power of TDC should be based on the heat generation of the real battery cell.

2.2. Preparation of battery module with cooling material

Fig. 3 illustrates the schematic diagram of a lab-scale battery module containing 16 dummy cells with pure PCM and copper foam-PCM. A layout of the 4 × 4 battery module is enclosed in a transparent acrylic box with an outer dimension of 130 mm × 130 mm × 70 mm and a wall thickness of 10 mm. The copper foam-PCM composite material was filled in the cell space. The thermophysical properties of the paraffin, copper foam, and aluminum are listed in Table 3. Commercial paraffin (PlusICE®) was utilized as the PCM with a phase change temperature of 40 °C. The copper foams with a pore density of 25 PPI and a porosity of 0.97 were applied to enhance heat transfer.

The preparation of copper foam-PCM material can be summarized in three steps. Firstly, the copper foam was cut into a specified dimension, and dummy cells were inserted into the hole of the skeleton of the copper foam (weight: 100 g). Subsequently, a certain amount of paraffin weighed by electric balancing and was poured into a beaker. The beaker was heated in a thermostatic water bath at 70 °C and stirred continuously until the PCM was completely melted. Finally, the melting paraffin is infiltrated into the pores of the copper foam for the preparation of the paraffin-copper foam composite material. The mass of paraffin perfused into the copper foam is approximately 332 g. The paraffin with an equivalent mass was poured into another battery module to prepare a pure PCM module. After the solidification of PCM, electrical connection and insulation protection was prepared. The ratio of PCM impregnated into the copper foam can be expressed as:

$$\sigma = \frac{m_{theo}}{m_{act}} = \frac{\varepsilon V \rho_{pcm}}{m_{act}} \tag{3}$$

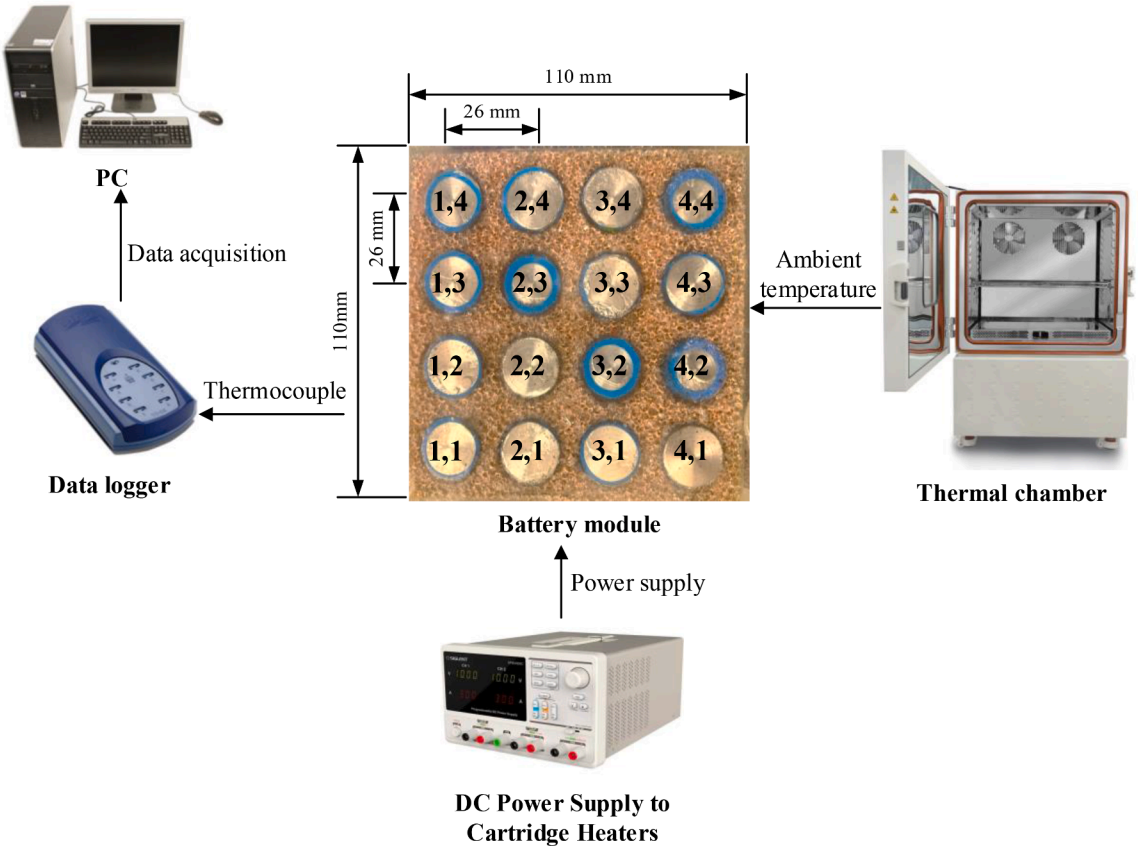

Fig. 4. Schematic diagram of the experimental setup.

where m_{theo}, m_{act}, and ρ_{pcm} denote the theoretical mass, actual mass, and density of PCM, respectively; ε and V denote the porosity of copper foam and total volume of composite material, respectively. Due to the high porosity of metal, the volume difference between copper foam-PCM and pure PCM is diminutive. The bottom acrylic plate is used to adjust the height of the material and ensure that the temperature sampling point is located in the middle of the material along the vertical direction. The mass of PCM determines the amount of heat absorbed, and can be expressed as [17]:

$$Q = m_{pcm}C_{pcm}(T_c - T_0) + m_{pcm}L$$

Q denotes the heat generation of the TDC. m_{pcm}, C_{pcm}, T_c, T_0 and L denote mass, heat capacity, phase change material, initial temperature, and latent heat of PCM, respectively.

2.3. Testing procedure

The experimental setup is shown in Fig. 4, which consists of the battery module, copper foam-PCM, K-type thermocouples, DC power supply (ROHDE&SCHWARS NGE100), and data acquisition equipment (Pico Technology TC-08), thermal imaging camera (FLIR T series), and a computer. Tests were conducted in a thermal chamber (Weiss Technik®) to maintain a constant ambient temperature (T_{amb}) with $a \pm 0.5$ °C fluctuation. A DC power supply was used to supply uninterrupted power for the electric cartridge heater. Temperature data were collected by a Picolog TC-08 data logger. K-type thermocouples were attached to the middle of each dummy cell surface to monitor their temperature. The thermal camera was fixed on the bottom of the acrylic box to record the temperature evolution of the battery module. Generally, the depth of discharge (DOD) of battery packs for electric vehicles is set between 40% and 60% [1]. The battery module test time is determined by the time needed to reach a 60% DOD. Average thermocouple readings are recorded at a time interval of 10 s. Since the decomposition temperature range of the solid interface (SEI) layer of the real battery cell is from 90 °C to 120 °C [48], the test will be stopped when the surface temperature of the battery reaches 90 °C. Three groups of experiments were conducted during various constant thermal power to evaluate the thermal performance of the BTMS with different cooling methods: 1) natural air cooling, 2) pure PCM, and 3) copper foam-PCM. The battery module was soaked in the thermal chamber for at least 24 h before the start of the tests. Two ambient temperatures (25 °C and 35 °C) were tested to evaluate the influence of ambient temperature on BTMS cooling performance. The scanning electron microscopy (SEM) image of copper foam and paraffin are shown in Appendix Fig. A1.

3. Results and discussion

This section consists of three sub-sections. The first one elaborates on the results of battery temperature evolution with air, PCM, and copper foam-PCM cooling. In the second section, the effects of different cooling strategies on temperature uniformity in the battery module are introduced. The third section evaluates the effects of copper foam-PCM passive cooling on the efficiency of cell-to-pack conversion.

3.1. Effects of different cooling methods on temperature rise

To better visualize the temperature evolution of the battery module, the cell temperature sampling can be classified into three categories by the layout of the centrosymmetric and axisymmetric battery module. Herein, the mean temperature of the cell located at (1,1) (1,4) (4,1) (4,4) is referred to as T1, the mean temperature of the cell located at (1,2) (1,3) (2,1) (3,1) (2,4) (3,4) (4,2) (4,3) is denoted as T2, and the mean temperature of the cell located at (2,2) (2,3) (3,2) (3,3) is represented by T3. Fig. 5 illustrates the temperature evolution curves of the battery

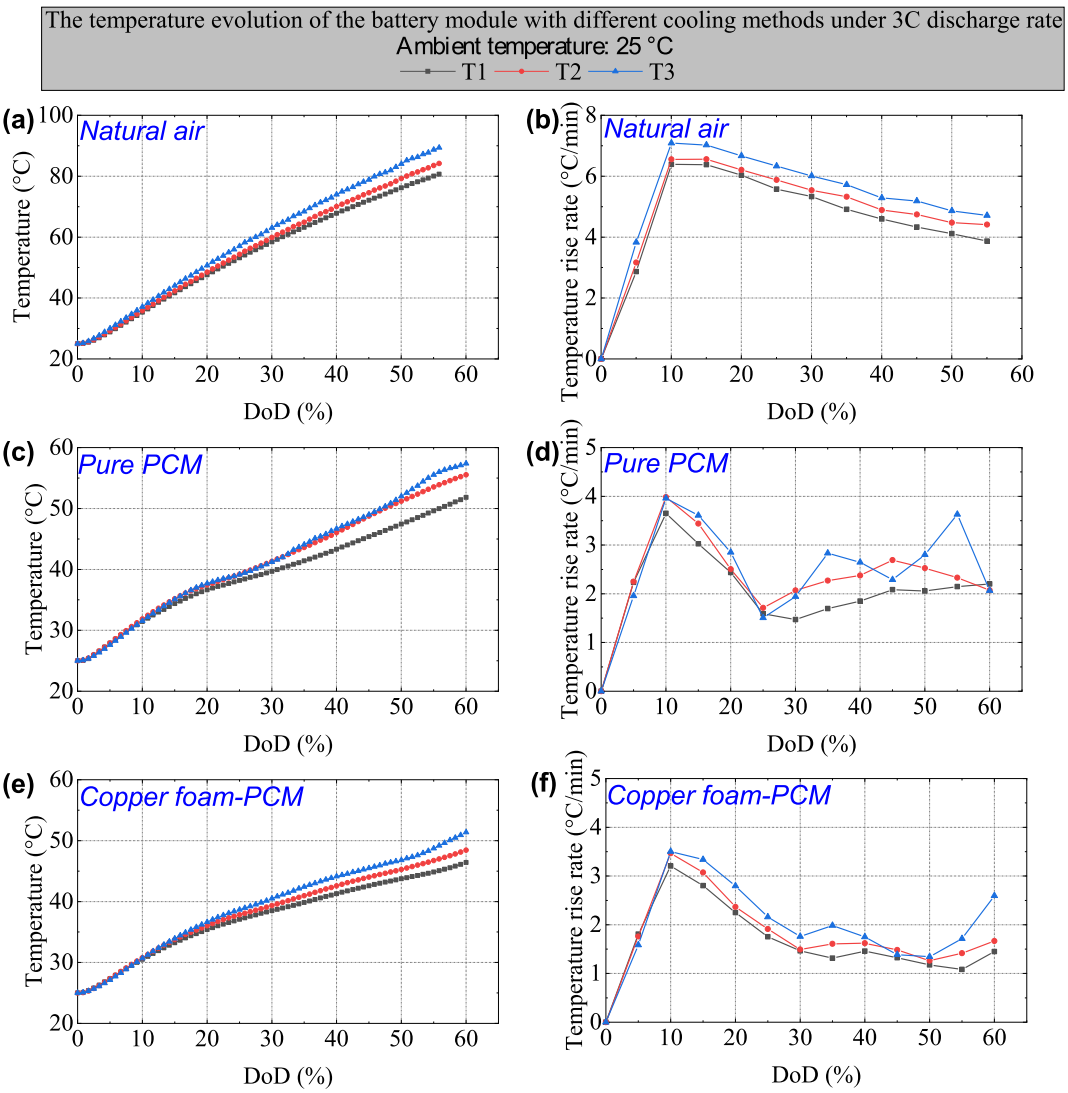

Fig. 5. Temperature curves and temperature rise rate of the battery module with different cooling methods under 3C discharge rate at T_{amb} = 25 °C: (a), (b) natural air cooling; (c), (d) pure PCM; (e), (f) copper foam-PCM.

module obtained by using different cooling methods under a 3C discharge rate at an ambient temperature of 25 °C. The temperature rise in the case of natural air cooling was found to be significantly higher than those in other cases. When the test ended, the temperature of the battery module with natural air cooling exceeded the safety temperature threshold (90 °C). The average temperature rise rate reached 5.3 °C/min in the case of natural air cooling. In the two cases of using PCM, there are similar temperature evolution curves. The temperatures of T3 in battery module with pure PCM and with copper foam-PCM reached 57.4 °C and 51.4 °C, respectively. During the test, the temperature rise rate of the battery module with pure PCM and with copper foam-PCM was consistently lower than 4 °C/min. In the melting process, PCM stores heat in the form of latent heat. Before PCM is melted, the temperature rise rate of the battery can be limited to less than 2 °C/min. During PCM melting, the temperature rise rate of the battery shows an increasing trend. After the complete melting of PCM, the heat is hindered from conversion into the phase change latent heat. Therefore, the temperature rise rate of the battery is accelerated, and the temperature rise rate at T3 exceeds 2 °C/min. The temperature curves of the battery module under other conditions are shown in Appendix Fig. A2-A7. Fig. 6 shows the impact of different cooling methods on battery temperature under the 3C discharge rate. As can be seen in the figure, the theoretical discharge time taken by the battery to reach the DOD of 60% at 3C current is 720 s. However, when natural air was used, the safe threshold temperature was triggered in advance. To evaluate the evolution of battery temperature over time when different cooling methods were applied, the duration of the comparative test with T_{amb} = 25 °C and T_{amb} = 35 °C were set to 560 s and 670 s, respectively. The temperature rise of T3 decreased by about 53% and 63% when pure PCM and copper foam-PCM were used than when natural air cooling was adopted, respectively. Table 4 list the comparison of the experimental results of this study with other reported literature on metal-based paraffin composites for BTMS. Based on the reported literature, the majority of research for cylindrical battery have chosen smaller cell capacities (2.5Ah-3.5Ah). However, there are considerable discrepancies between the discharge currents of different capacity batteries at the same discharge rate. This paper focuses on the examination of the temperature evolution of high-capacity cylindrical batteries at higher ambient temperatures.

Fig. 7 shows the plot of the temperature difference between pure PCM and copper foam-PCM at the end of the 3C discharge rate test. Compared with pure PCM, the temperature of T1, T2, and T3 in the battery module using copper foam-PCM were reduced by 5.4 °C, 6.6 °C, and 6 °C under 3C discharging rate and T_{amb} = 25 °C, respectively. Based on Wang et al. [54] examining the degradation test of NMC LiBs, high temperatures will accelerate the cycle life loss of LiBs. Therefore, copper

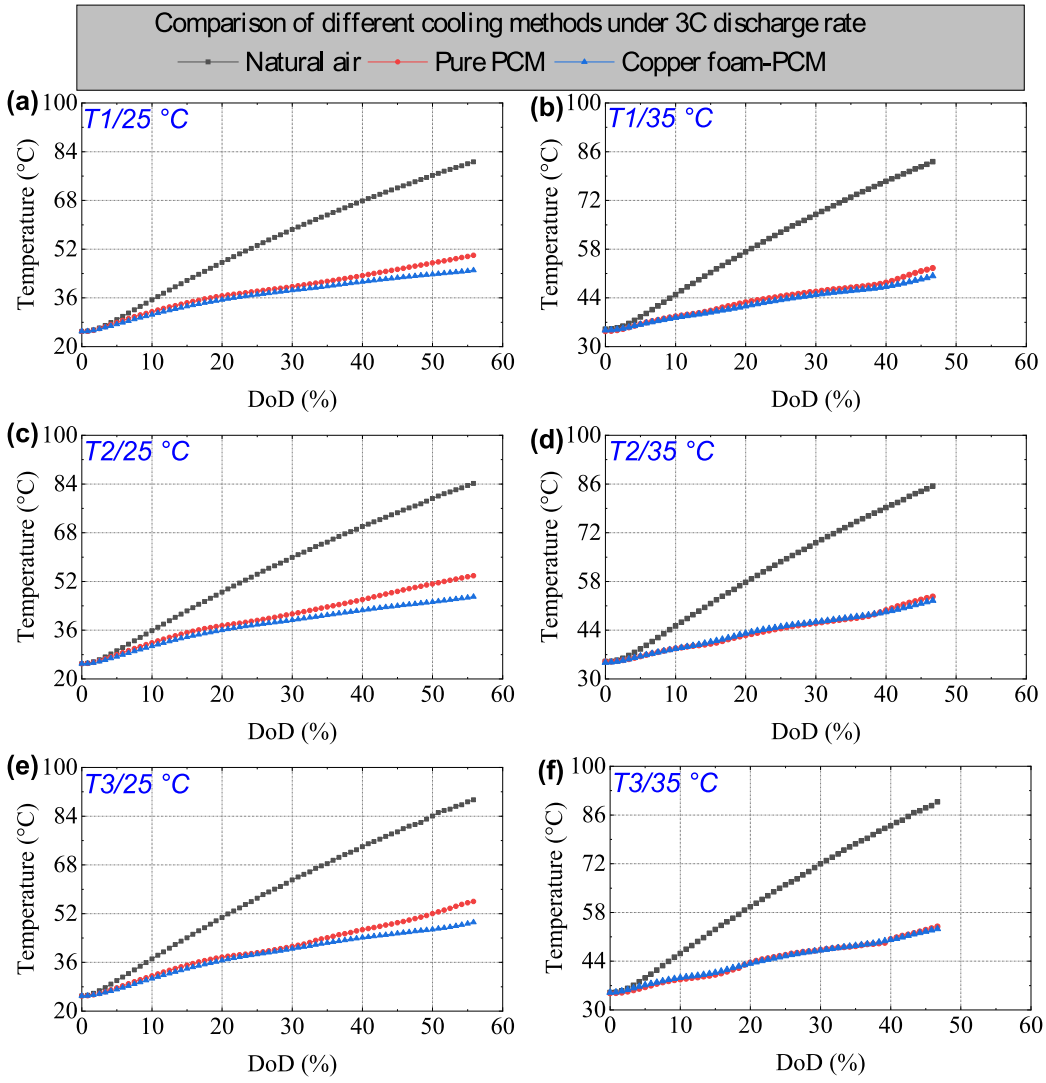

Fig. 6. The influence of different cooling methods on battery temperature under 3C discharge rate: (a) T1, T_{amb} = 25 °C; (b) T1, T_{amb} = 35 °C; (c) T2, T_{amb} = 25 °C; (d) T2, T_{amb} = 35 °C;(e) T3, T_{amb} = 25 °C; (f) T3, T_{amb} = 35 °C.

Table 4
Summary of passive cooling paraffin composite material for BTMS.

	Battery capacity (Ah)	Battery Load	Strategy	Melting temp. (°C)	Latent heat (kJ/kg)	Ambient temp. (°C)	Maximum temp. (°C)
Azizi et al. [49],	3	3C	Aluminum wire mesh	56	195	26	46.5
Zhao et al., [31]	3.4	2C	Copper foam	34–36	210	25	42
Hussain et al. [50],	3.4	2C	Nickel foam	38–41	–	25	45
Pan et al., [51]	2.9	2.4C	Copper fiber	48–50	–	30	51.2
Luo et al., [52]	2.6	4C	EG	34	222	20	35
This study	4.8	3C	Copper foam	40	137	25/35	51.4/59.6

Table 5
Parameters for GCTP and VCTP calculation [53].

Parameters	Values
SE_{cell}	900 kJ/kg
η	90%
T_c	35 °C
T_{amb}	25 °C
$f_{periphery}$	36%

foam-PCM cooling can mitigate the degradation of LiBs induced by temperature rise.

3.2. Effects of different cooling methods on temperature uniformity

Temperature uniformity in the battery module is regarded as a significant indicator in evaluating the effectiveness of cooling methods. To ensure both battery performance and safety, the temperature difference between batteries in the module should be restricted to 5 °[18]. Fig. 8 shows the maximum temperature difference in the module with different cooling methods at the end of the test. The temperature

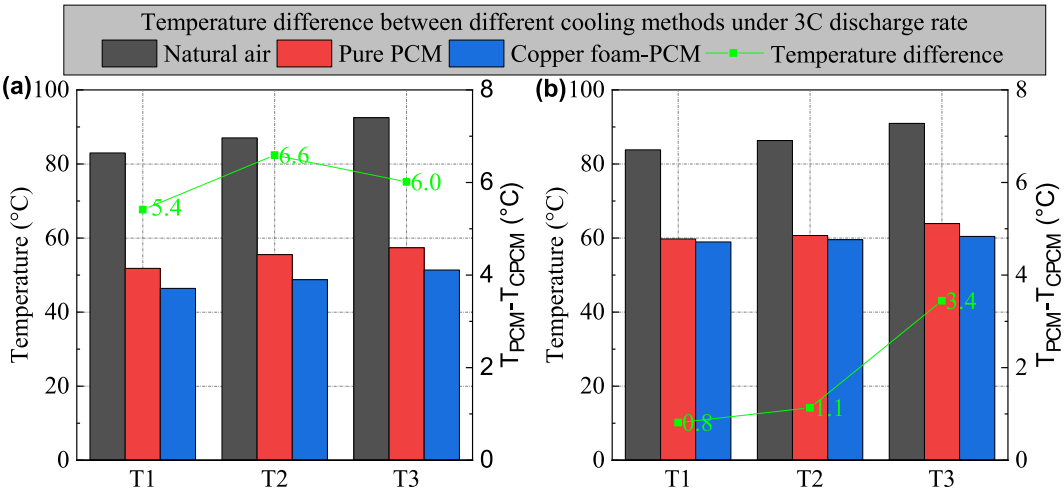

Fig. 7. Temperature difference between different cooling methods at the end of 3C discharge rate test: (a) T_{amb} = 25 °C; (b) T_{amb} = 35 °C.

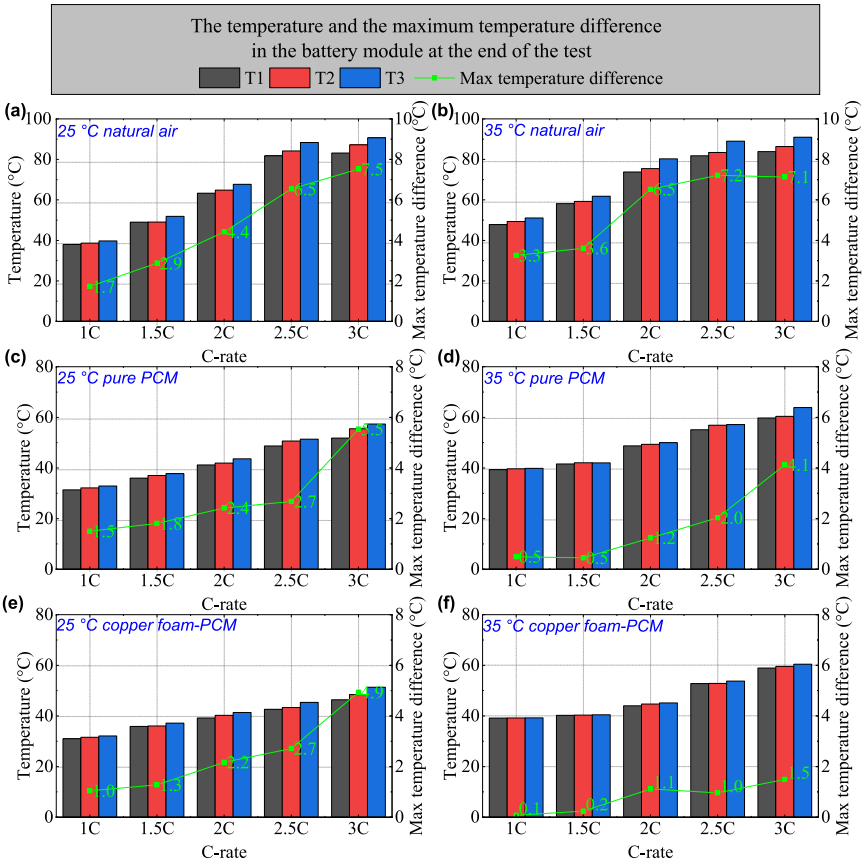

Fig. 8. Maximum temperature difference between the selected cells in the module at the end of the test: (a) natural air convection, T_{amb} = 25 °C; (b) natural air convection, T_{amb} = 35 °C; (c) pure PCM cooling, T_{amb} = 25 °C; (d) pure PCM cooling, T_{amb} = 35 °C; (e) copper foam-PCM cooling, T_{amb} = 25 °C; (f) copper foam-PCM cooling, T_{amb} = 25 °C.

difference between battery cells shows a positive correlation with the discharge rate. As for the maximum temperature difference in the battery module with natural air cooling, it reached 7.5 °C at T_{amb} = 25 °C and 3C discharge rate. Compared with natural air cooling, the temperature uniformity of the battery module was better maintained by using PCM, especially in case of a high discharge rate. Copper foam, as a high-temperature-resistant porous frame, can perform well in confining PCM in the pores to prevent the occurrence of non-uniformity temperature distribution caused by the flow of melted PCM. The temperature differential in the battery module using copper foam-PCM was lower than that of pure PCM, which was limited to within 5 °C. Cavalheiro et al. [55] indicated that large non-uniform temperature distribution in the battery module deteriorates the degradation non-uniformity of LiBs. Copper foam-PCM can maintain temperature uniformity between battery cells thereby improving the degradation non-uniformity. In the case of PCM and copper foam-PCM, the temperature difference between cells at T_{amb} = 35 °C is lower than that at T_{amb} = 25 °C. The possible causes of this phenomenon are that the local melting of PCM causes temperature

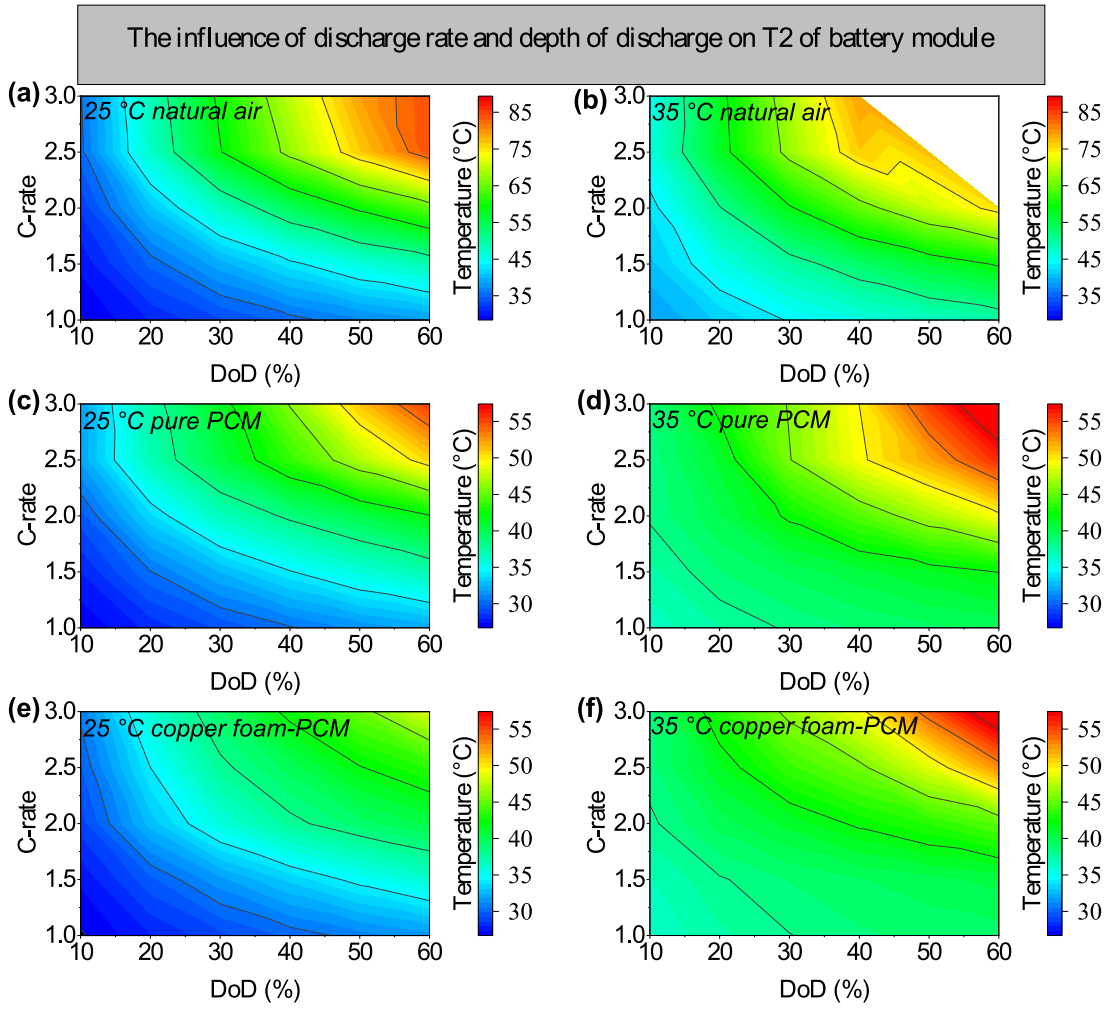

Fig. 9. Effects of discharge rate and depth of discharge on temperature evolution of battery module: (a) natural air, T_{amb} = 25 °C; (b) natural air, T_{amb} = 35 °C; (c) pure PCM, T_{amb} = 25 °C; (d) pure PCM, T_{amb} = 35 °C; (e) copper foam-PCM, T_{amb} = 25 °C; (f) copper foam-PCM, T_{amb} = 35 °C.

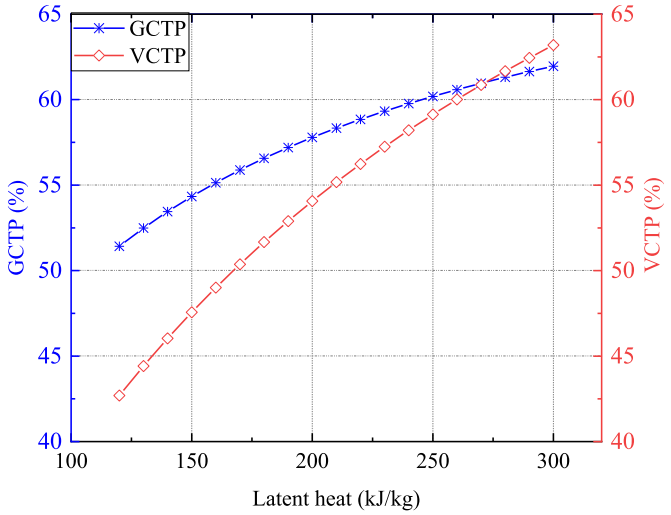

Fig. 10. GCTP and VCTP of the battery pack under various latent heat of PCM.

non-uniformity distribution at T_{amb} = 25 °C. On the contrary, due to the phase change temperature of PCM material being 40 °C, PCM may have completely melted at the end of the battery discharge at T_{amb} = 35 °C, resulting in a lower temperature difference between cells but a higher temperature rise of battery module compare to the case at T_{amb} = 25 °C. The temperature fields of the battery module, as captured by the thermal imaging camera, are shown in Appendix Fig. A8.

Fig. 9 illustrates the impact of DOD and discharge rate on the battery

module temperature in the T2 position. The battery temperature shows an upward trend with the increase in discharge rate and DOD. A large temperature gradient is observed in the battery module with natural air cooling under the high C-rate and DOD. In comparison with natural air cooling, the temperature rise of the case using PCM has a lower temperature rise affected by discharge rate and DOD. In addition, ambient temperature has a significant impact in the case of using PCM cooling. When the ambient temperature approaches the melting point of the PCM, the heat absorbed from the battery during phase change diminishes. The cooling performance of pure PCM deteriorates considerably, given the high ambient temperature. Therefore, copper foam with high-temperature resistance and high thermal conductivity is added to improve the thermal conductivity of PCM and enhance the heat dissipation performance of composite material. Copper foam-PCM cooling shows a massive potential to inhibit temperature rise for battery modules. Effects of discharge rate and depth of discharge on battery modules with different positions are shown in Appendix Fig. A9-11.

3.3. Cell-to-pack conversion efficiency

Thermal management systems significantly influence the weight and volume of battery packs. To demonstrate the feasibility of the copper foam-PCM cooling in practical application, the cell-to-pack conversion efficiency is taken into account to evaluate the impact of this method on the energy density of the battery pack, including the ratio of cell-to-pack energy density on a gravimetric (GCTP) or volumetric (VCTP) basis. The average GCTP and VCTP of commercial battery packs are about 55% and 50%, respectively [53]. However, commercial battery packs are mostly active cooling, which will cause parasitic power consumption. As a sort of passive thermal management solution, the copper foam-PCM composite material cooling can be effective in addressing the parasitic power, reliability, and space consumption of the auxiliary components caused by active thermal management. The specific energy (SE) of the 21,700 NMC battery is obtained based on the battery capacity and nominal voltage. The parameters for GCTP and VCTP calculation are listed in Table 4.

The specific heat capacity of copper foam-PCM composite material can be calculated as the following equation:

$$c_{p,CPCM} = c_{p,PCM}\frac{m_{PCM}}{m_{CPCM}} + c_{p,CF}\frac{m_{CF}}{m_{CPCM}} \tag{4}$$

Considering the sensible heat absorbed by PCM and battery when their temperature is raised from the ambient temperature to the operating temperature. GCTP and VCTP of BTMS with copper foam-PCM cooling can be estimated as follows [53]:

$$GCTP = \frac{SE_{pack}}{SE_{cell}} = \left(1 + \frac{SE_{cell}(1-\eta) - c_{p,cell}(T_c - T_{amb})}{\lambda_{CPCM} + c_{p,CPCM}(T_c - T_{amb})} + f_{periphery}\right)^{-1} \tag{5}$$

$$VCTP = \frac{SE_{pack}}{SE_{cell}} = \left[1 + \left(\frac{SE_{cell}(1-\eta) - c_{p,cell}(T_c - T_{amb})}{\lambda_{CPCM} + c_{p,CPCM}(T_c - T_{amb})}\right)\left(\frac{\rho_{cell}}{\rho_{CPCM}}\right)\right]^{-1} \tag{6}$$

where λ and c represent latent heat of PCM and specific heat capacity, respectively; SE denotes specific energy; η represents energy efficiency for the electrical vehicle; $f_{periphery}$ represents the ratio of periphery mass (cables, pack housing, electronics, etc.) to cell mass; T_c and T_{amb} represent battery surface temperature and ambient temperature, respectively.

GCTP and VCTP efficiency reach 53.1% and 45.6% for the battery pack with copper foam-PCM, respectively. Although the GCTP of battery packs using this composite material is slightly lower than the average value of commercial battery packs for vehicles, the elimination of parasitic power can improve the electric vehicle energy consumption and indirectly increase the energy density of the battery pack. Fig. 10. GCTP and VCTP of the battery pack under various latent heat Fig. 10 shows the GCTP and VCTP of the battery pack under various latent heat. Based on Eqs. (5) and (6), the increase of PCM latent heat can effectively reduce the proportion of the BTMS in the volume and mass of the battery pack.

4. Conclusion

In this study, BTMS with passive copper foam-PCM cooling was explored experimentally and compared to two other cooling methods (natural air cooling and pure PCM). Based on the thermal characteristics of LiBs, a battery module containing 16 thermal dummy cells was built to replace real cells for the experiment. Cell temperature was monitored at various discharge rates to assess the heat dissipation performance of thermal management solutions. The main findings drawn from this study are listed as follows:

- The copper foam-PCM composite material can effectively can effectively mitigate the rapid temperature rise of a battery cell during high charge/discharge rate. At a 3C discharge rate, the maximum temperature rise of cases utilizing copper foam-PCM dropped from 57.4 °C to 51.4 °C when compared to pure PCM.
- The copper foam-PCM composite material outperforms pure PCM in enhancing the temperature uniformity of the battery module. The maximum temperature differential in the battery module employing copper foam-PCM was constrained to less than 5 °C at the discharge rate of 3C.
- The cell-to-pack ratio is introduced to evaluate the influence imposed by BTMS on the mass and volume of the battery pack. The GCTP and VCTP battery modules using copper foam-PCM cooling reach 53.1% and 45.6%, respectively. The improvement of the cell-to-pack ratio of the battery pack can be realized by selecting a PCM with higher latent heat.

Future work

Based on the abovementioned findings, the copper foam-PCM cooling is still worthy of further optimization in terms of lightweight. The temperature of the battery module with copper foam-PCM approached 60 °C at the end of the 3C discharge rate. Therefore, passive cooling has limitations for the heat dissipation performance of the battery module at high C-rates (5C or 10 C). In the future, the authors will examine the active-passive thermal management solution to reduce the temperature rise of LiBs at the higher C-rate. The author also will further perform the optimization of the battery thermal management system through the incorporation of numerical simulation and experimental validation. The real battery test will be implemented for the development of battery thermal management to examine the thermal behavior of the battery under various operating conditions, such as the driving cycle and extreme thermal runaway conditions, etc.

Declaration of Competing Interest

The authors declare that they have no known competing financial interests or personal relationships that could have appeared to influence the work reported in this paper.

Data availability

Data will be made available on request.

Appendix

Fig A1-Fig A11

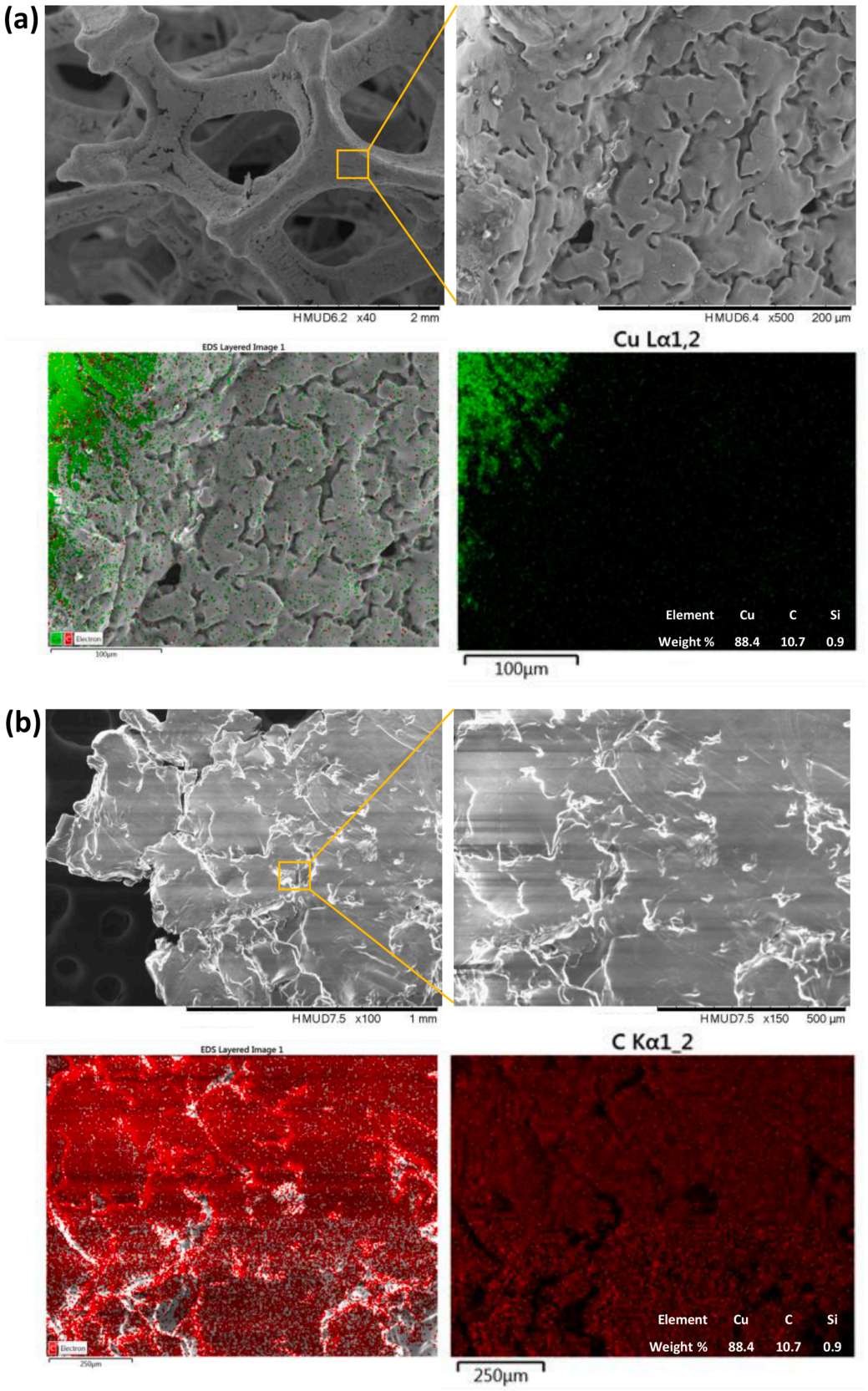

Fig. A1. SEM images of cooling materials: (a) copper foam; (b) paraffin.

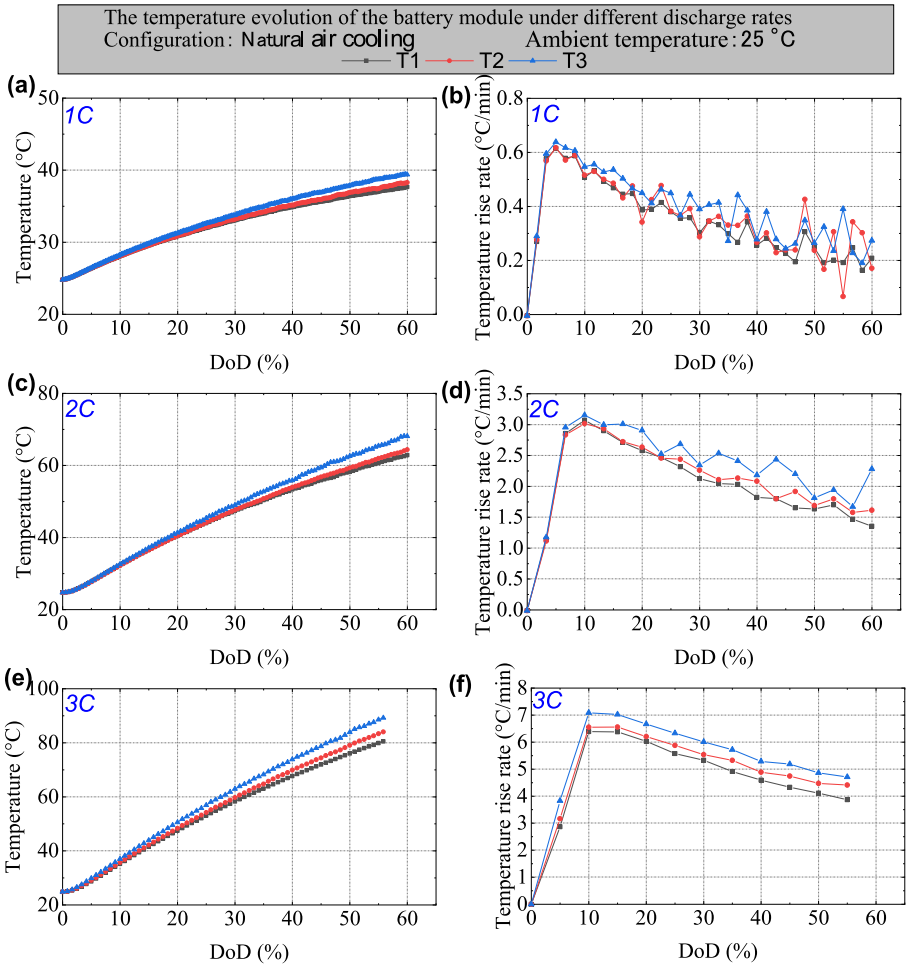

Fig. A2. Temperature curves of the battery module under natural air cooling at T_{amb} = 25 °C: (a) temperature evolution of battery at 1C; (b) temperature rise rate of battery at 1C; (c) temperature evolution of battery at 2C; (d) temperature rise rate of battery at 2C; (e) temperature evolution of battery at 3C; (f) temperature rise rate of battery at 3C.

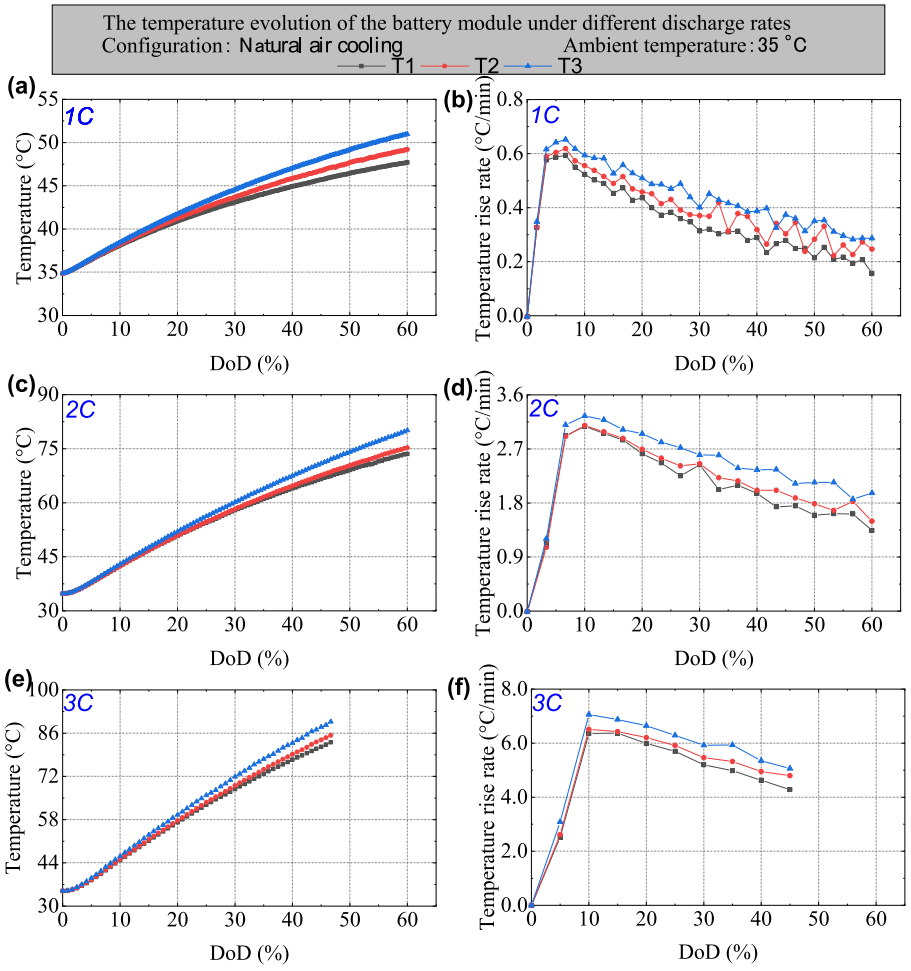

Fig. A3. Temperature curves of the battery module under natural air cooling at T_{amb} = 35 °C: (a) temperature evolution of battery at 1C; (b) temperature rise rate of battery at 1C; (c) temperature evolution of battery at 2C; (d) temperature rise rate of battery at 2C; (e) temperature evolution of battery at 3C; (f) temperature rise rate of battery at 3C.

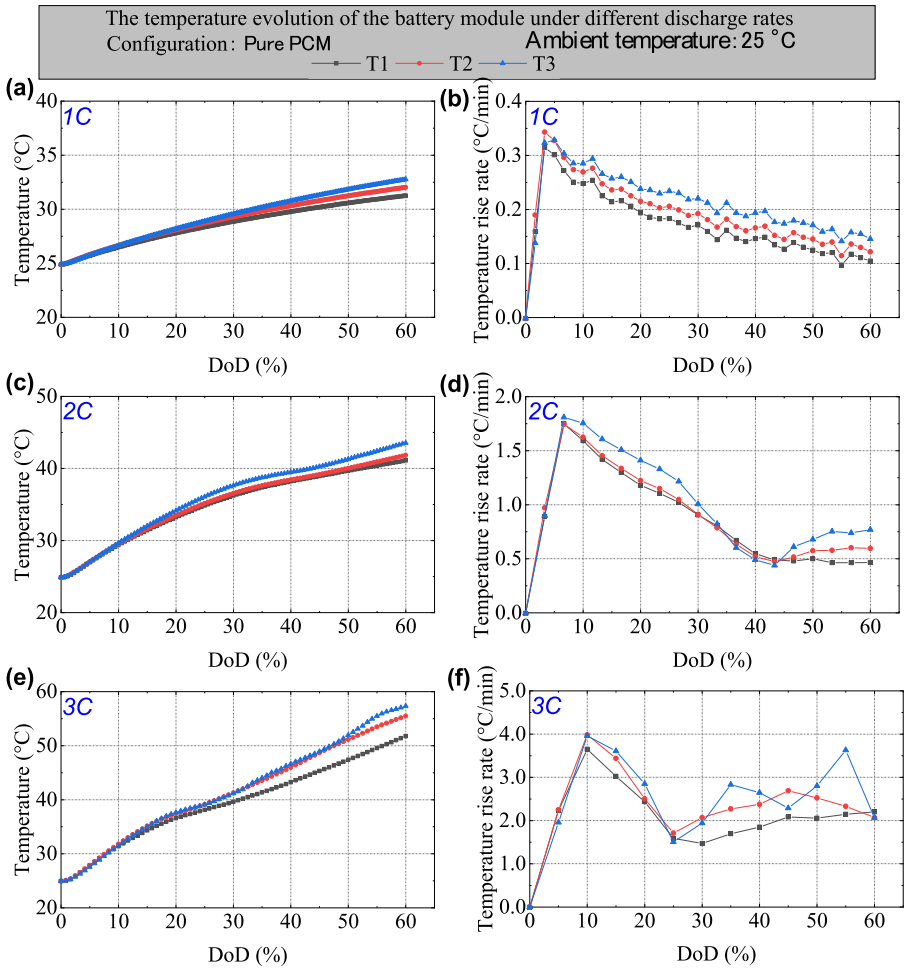

Fig. A4. Temperature curves of the battery module under pure PCM cooling at $T_{amb} = 25$ °C: (a) temperature evolution of battery at 1C; (b) temperature rise rate of battery at 1C; (c) temperature evolution of battery at 2C; (d) temperature rise rate of battery at 2C; (e) temperature evolution of battery at 3C; (f) temperature rise rate of battery at 3C.

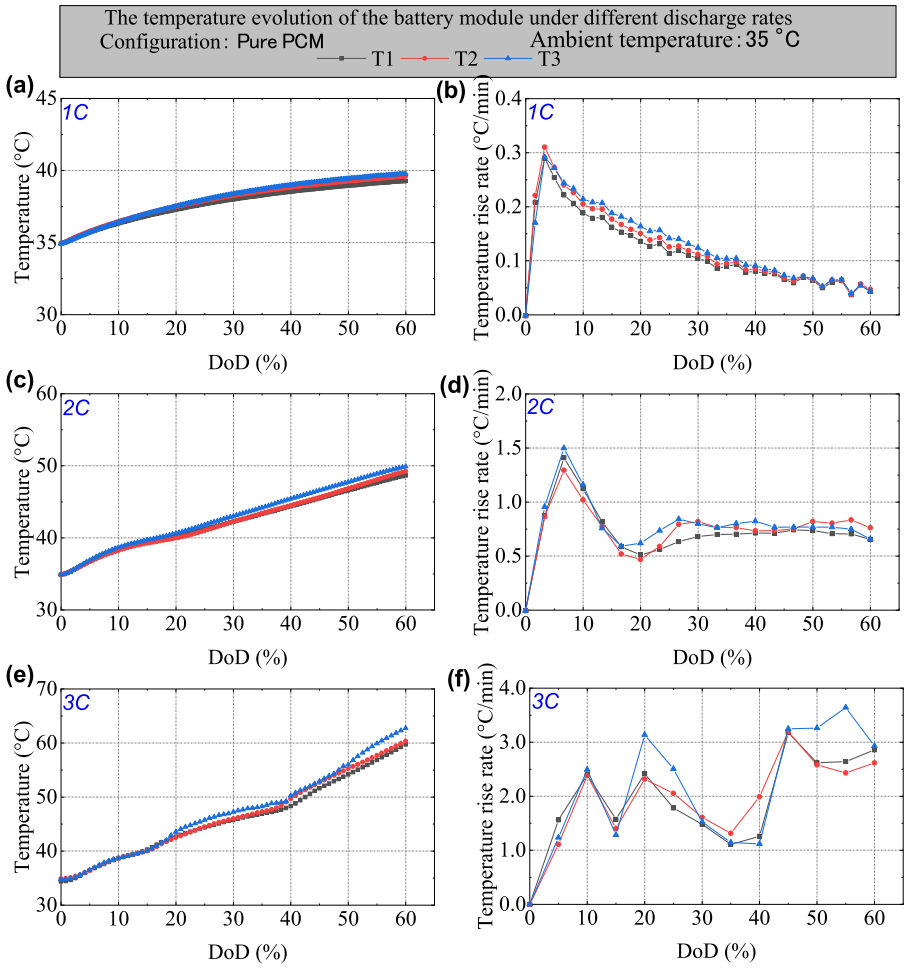

Fig. A5. Temperature curves of the battery module under pure PCM cooling at $T_{amb} = 35$ °C: (a) temperature evolution of battery at 1C; (b) temperature rise rate of battery at 1C; (c) temperature evolution of battery at 2C; (d) temperature rise rate of battery at 2C; (e) temperature evolution of battery at 3C; (f) temperature rise rate of battery at 3C.

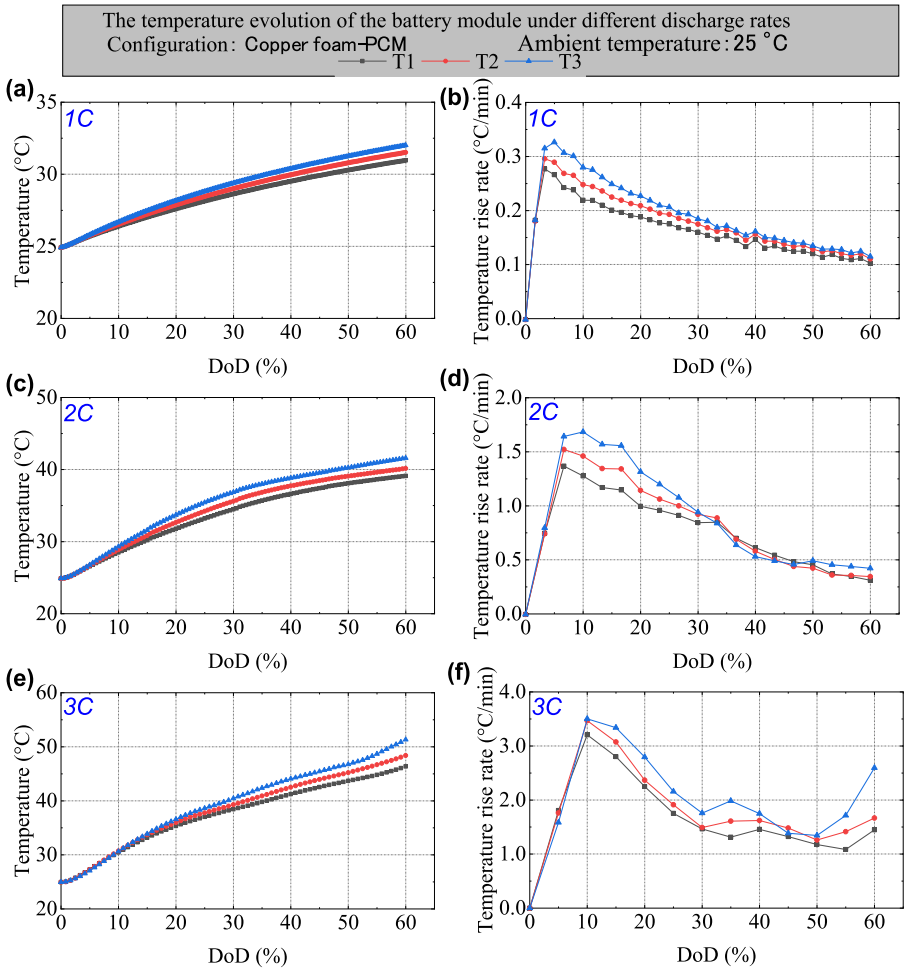

Fig. A6. Temperature curves of the battery module under copper foam-PCM cooling at T_{amb} = 35 °C: (a) temperature evolution of battery at 1C; (b) temperature rise rate of battery at 1C; (c) temperature evolution of battery at 2C; (d) temperature rise rate of battery at 2C; (e) temperature evolution of battery at 3C; (f) temperature rise rate of battery at 3C.

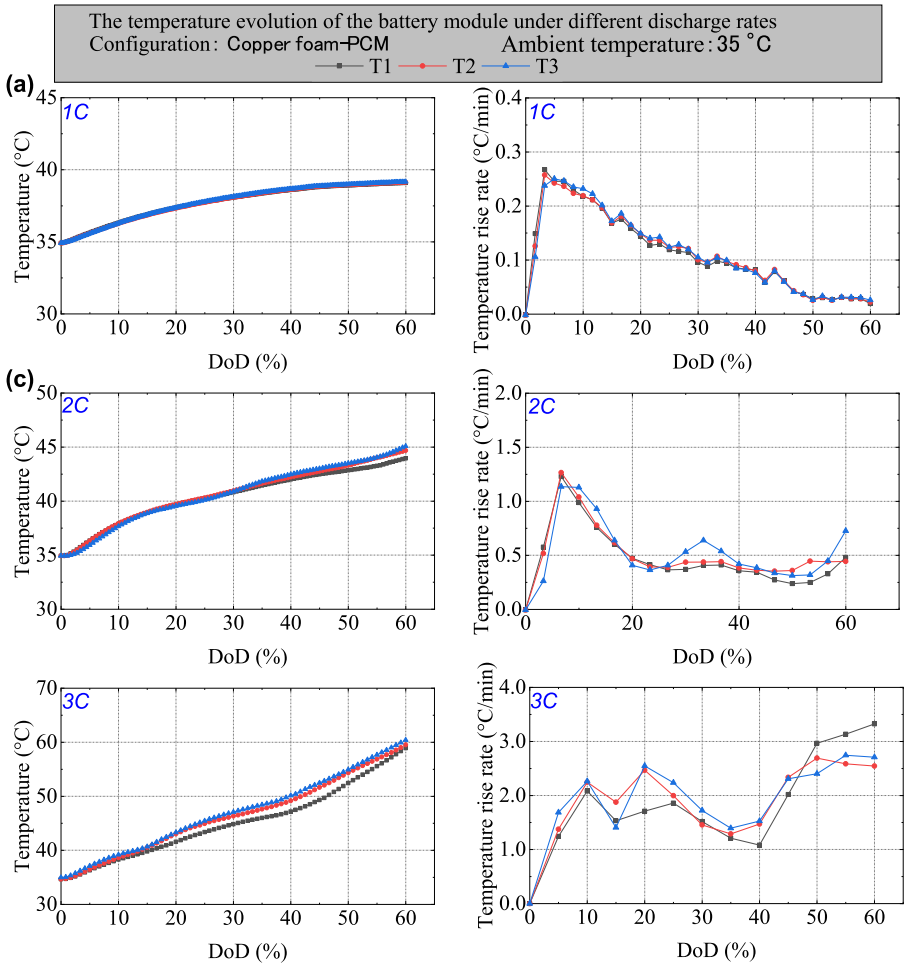

Fig. A7. Temperature curves of the battery module under copper foam-PCM cooling at $T_{amb} = 35$ °C: (a) temperature evolution of battery at 1C; (b) temperature rise rate of battery at 1C; (c) temperature evolution of battery at 2C; (d) temperature rise rate of battery at 2C; (e) temperature evolution of battery at 3C; (f) temperature rise rate of battery at 3C.

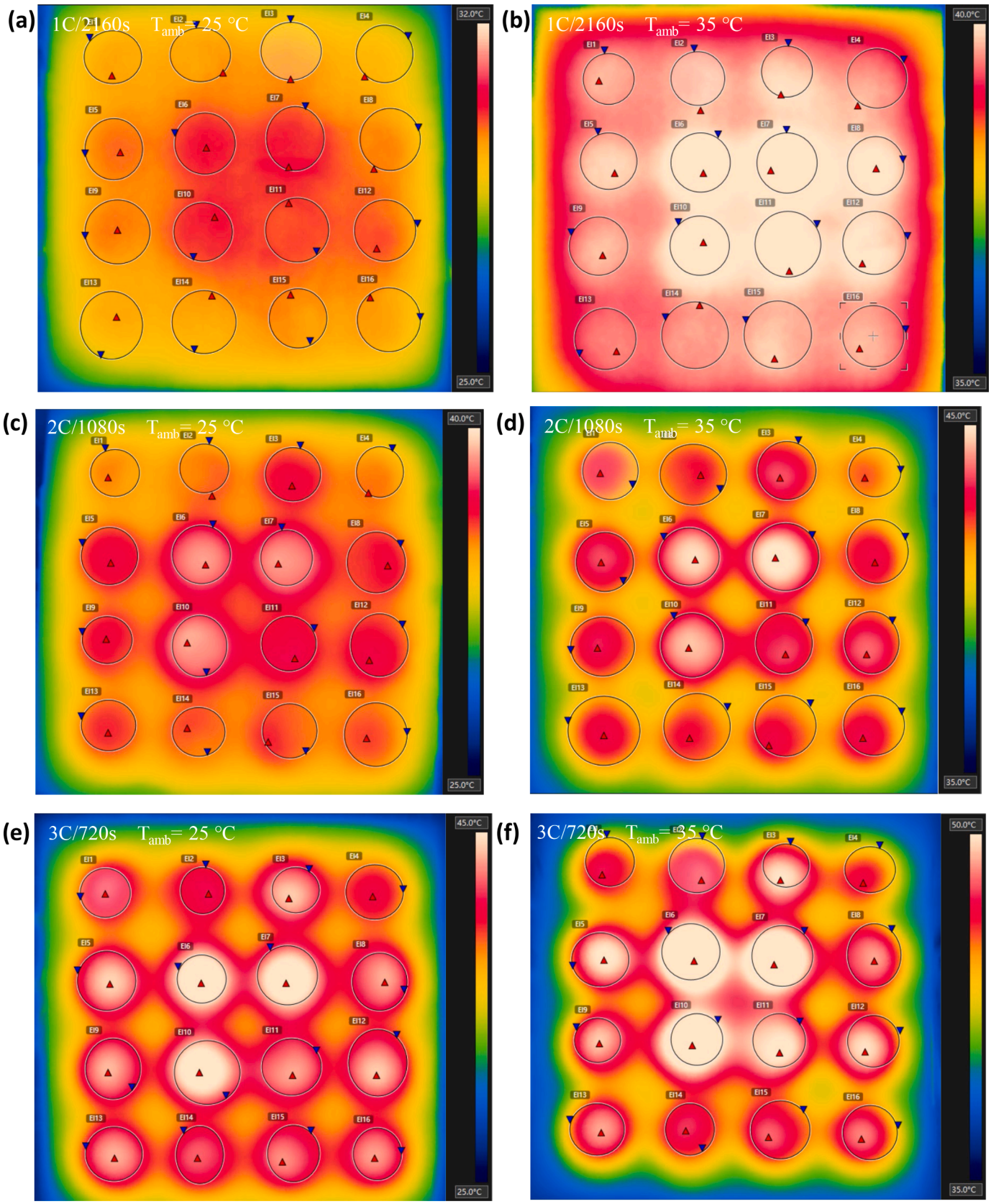

Fig. A8. The recorded infrared imagery of module under different discharge rate: (a) 1C,T_{amb} = 25 °C; (b) 1C,T_{amb} = 35 °C; (c) 2C,T_{amb} = 25 °C; (d) 2C,T_{amb} = 35 °C; (e) 3C,T_{amb} = 25 °C; (f) 3C,T_{amb} = 35 °C.

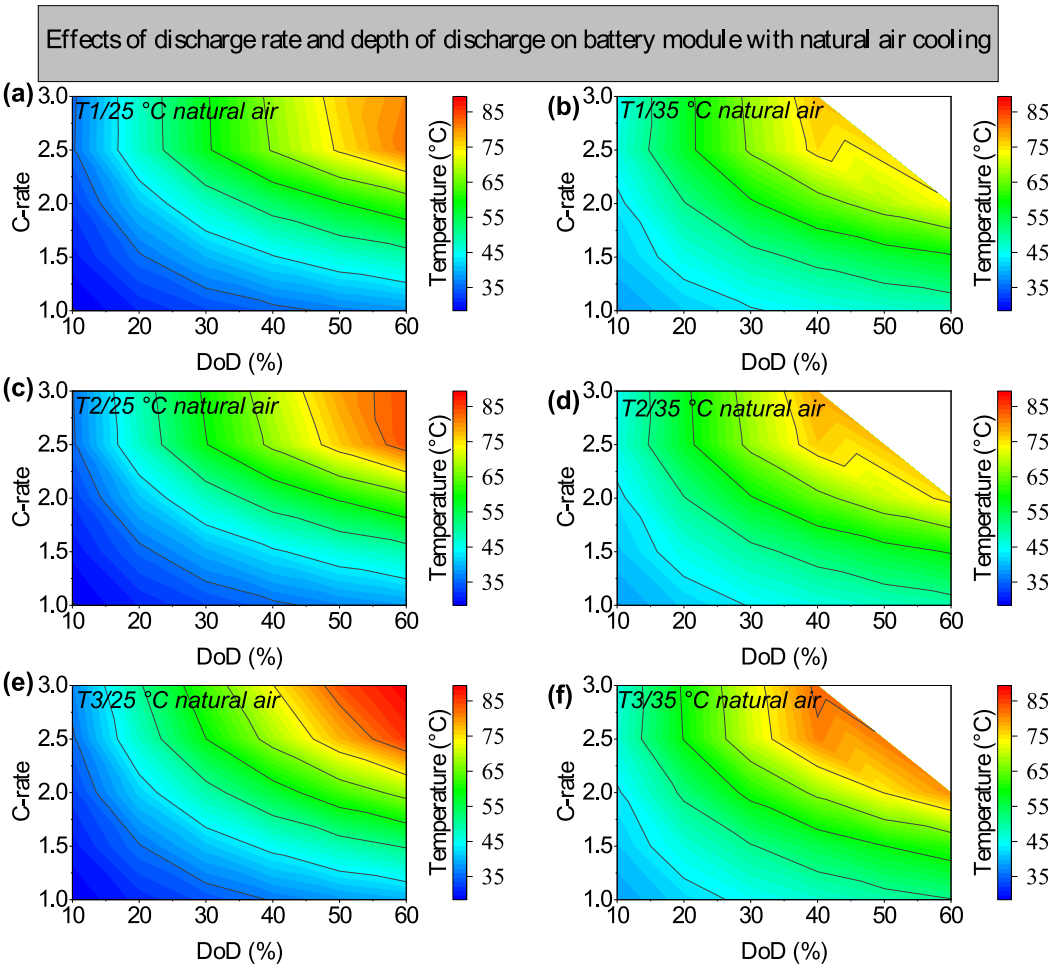

Fig. A9. Effects of discharge rate and depth of discharge on battery module with natural air: (a) T1, T_{amb} = 25 °C; (b) T2, T_{amb} = 35 °C; (c) T3, T_{amb} = 25 °C; (d) T1, T_{amb} = 35 °C; (e) T2, T_{amb} = 25 °C; (f) T3, T_{amb} = 35 °C.

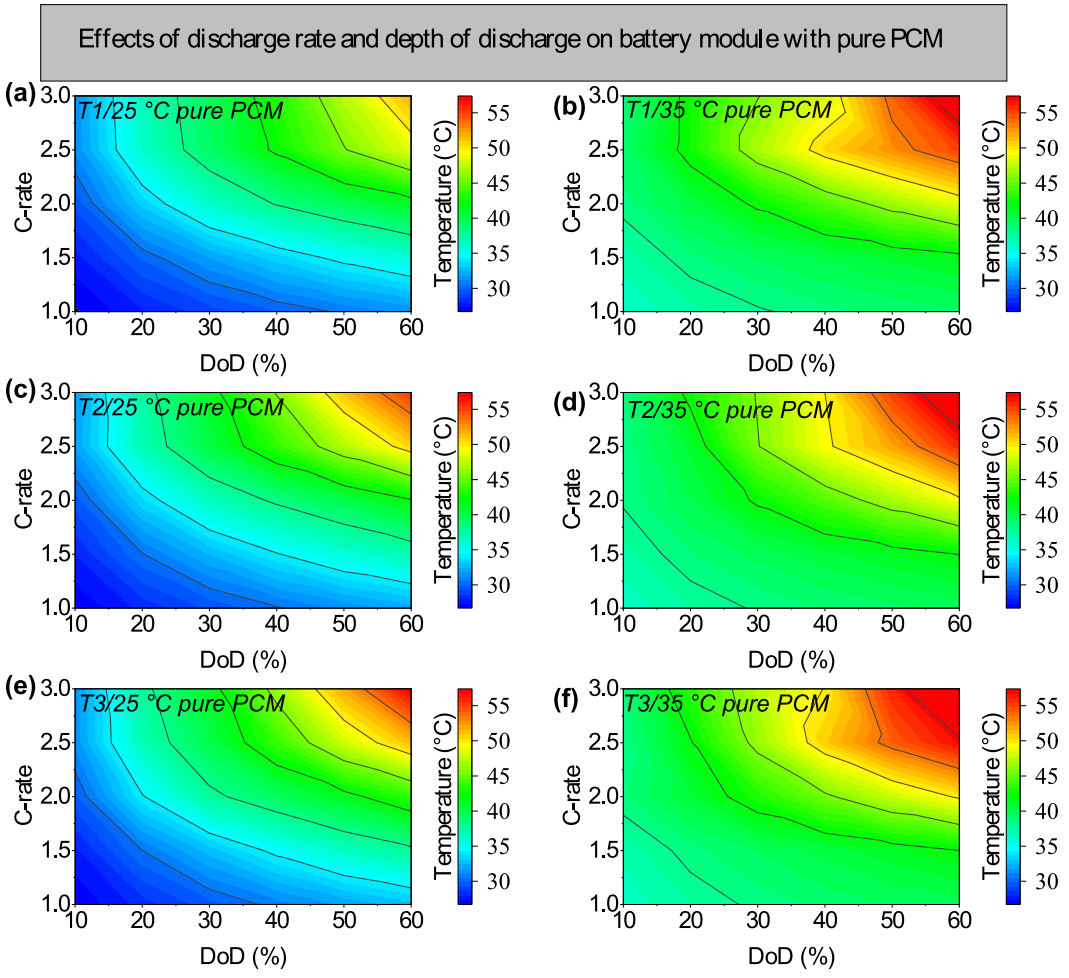

Fig. A10. Effects of discharge rate and depth of discharge on battery module with pure PCM: (a) T1, T_{amb} = 25 °C; (b) T2, T_{amb} = 35 °C; (c) T3, T_{amb} = 25 °C; (d) T1, T_{amb} = 35 °C; (e) T2, T_{amb} = 25 °C; (f) T3, T_{amb} = 35 °C.

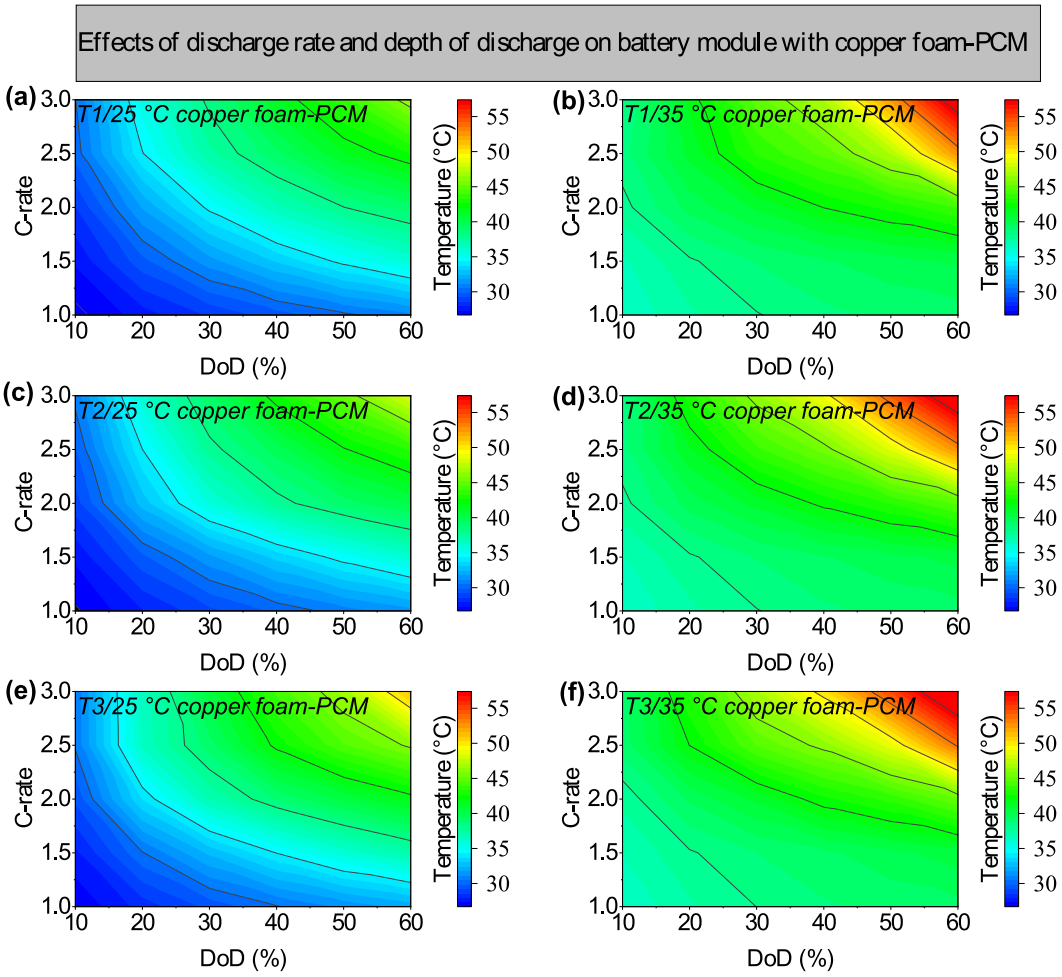

Fig. A11. Effects of discharge rate and depth of discharge on battery module with copper foam-PCM: (a) T1, T_{amb} = 25 °C; (b) T2, T_{amb} = 35 °C; (c) T3, T_{amb} = 25 °C; (d) T1, T_{amb} = 35 °C; (e) T2, T_{amb} = 25 °C; (f) T3, T_{amb} = 35 °C.

References

[1] Q. Zhou, et al., Multi-step reinforcement learning for model-free predictive energy management of an electrified off-highway vehicle, Appl. Energy 255 (2019), 113755, https://doi.org/10.1016/j.apenergy.2019.113755.

[2] S. Su, W. Li, Y. Li, A. Garg, L. Gao, Q. Zhou, Multi-objective design optimization of battery thermal management system for electric vehicles, Appl. Therm. Eng. 196 (2021), 117235, https://doi.org/10.1016/j.applthermaleng.2021.117235.

[3] S.H. Hong, D.S. Jang, S. Park, S. Yun, Y. Kim, Thermal performance of direct two-phase refrigerant cooling for lithium-ion batteries in electric vehicles, Appl. Therm. Eng. 173 (March) (2020), 115213, https://doi.org/10.1016/j.applthermaleng.2020.115213.

[4] A. Verma, S. Shashidhara, D. Rakshit, A comparative study on battery thermal management using phase change material (PCM, Therm. Sci. Eng. Prog. 11 (2019) 74–83, https://doi.org/10.1016/j.tsep.2019.03.003.

[5] X. Feng, M. Ouyang, X. Liu, L. Lu, Y. Xia, X. He, Thermal runaway mechanism of lithium ion battery for electric vehicles: a review, Energy Storage Mater. 10 (December 2016) (2018) 246–267, https://doi.org/10.1016/j.ensm.2017.05.013.

[6] G. Xia, L. Cao, G. Bi, A review on battery thermal management in electric vehicle application, J. Power Sources 367 (2017) 90–105, https://doi.org/10.1016/j.jpowsour.2017.09.046.

[7] Z. Shi, G. Chen, L. Zhu, J. Li, Y. Xia, Sandwich structure design of a cooling fin for battery modules against impact loads, Automot. Innov. 3 (3) (2020) 260–269, https://doi.org/10.1007/s42154-020-00107-z.

[8] F. Chen, et al., Air and PCM cooling for battery thermal management considering battery cycle life, Appl. Therm. Eng. 173 (2020), https://doi.org/10.1016/j.applthermaleng.2020.115154.

[9] B. Li, et al., Thermal management of electrified propulsion system for low-carbon vehicles, Automotive Innovation 3 (4) (2020) 299–316, https://doi.org/10.1007/s42154-020-00124-y.

[10] M. Shen, Q. Gao, Simulation and analysis of dual-evaporator refrigeration system for electric vehicles, Automot. Innov. 3 (4) (2020) 347–355, https://doi.org/10.1007/s42154-020-00115-z.

[11] R. Huang, Z. Li, W. Hong, Q. Wu, X. Yu, Experimental and numerical study of PCM thermophysical parameters on lithium-ion battery thermal management, Energy Reports 6 (2020) 8–19, https://doi.org/10.1016/j.egyr.2019.09.060.

[12] C. Yao, et al., Thermal performance of a micro heat pipe array for battery thermal management under special vehicle-operating conditions, Automot. Innov. 3 (4) (2020) 317–327, https://doi.org/10.1007/s42154-020-00114-0.

[13] Q. Zhou, W. Zhang, S. Cash, O. Olatunbosun, H. Xu, G. Lu, Intelligent sizing of a series hybrid electric power-train system based on Chaos-enhanced accelerated particle swarm optimization, Appl. Energy 189 (2017) 588–601, https://doi.org/10.1016/j.apenergy.2016.12.074.

[14] P. Dubey, G. Pulugundla, A.K. Srouji, Direct comparison of immersion and cold-plate based cooling for automotive li-ion battery modules, Energies 14 (5) (2021), https://doi.org/10.3390/en14051259.

[15] A.G. Olabi, et al., Battery thermal management systems: recent progress and challenges, Int. J. Thermofluids 15 (2022), 100171, https://doi.org/10.1016/j.ijft.2022.100171.

[16] H. Jouhara, N. Serey, N. Khordehgah, R. Bennett, S. Almahmoud, S.P. Lester, Investigation, development and experimental analyses of a heat pipe based battery thermal management system, Int. J. Thermofluids 1–2 (2020), 100004, https://doi.org/10.1016/j.ijft.2019.100004.

[17] F. Chen, et al., Air and PCM cooling for battery thermal management considering battery cycle life, Appl. Therm. Eng. 173 (October 2019) (2020), 115154, https://doi.org/10.1016/j.applthermaleng.2020.115154.

[18] G. Wang, Q. Gao, Y. Yan, Y. Wang, Thermal management optimization of a lithium-ion battery module with graphite sheet fins and liquid cold plates, Automot. Innov. 3 (4) (2020) 336–346, https://doi.org/10.1007/s42154-020-00121-1.

[19] Z. Li, et al., Applications and technological challenges for heat recovery, storage and utilisation with latent thermal energy storage, Appl. Energy 283 (2021), 116277, https://doi.org/10.1016/j.apenergy.2020.116277.

[20] Y. Zhao, et al., Expanded graphite – Paraffin composite phase change materials: effect of particle size on the composite structure and properties, Appl. Therm. Eng. 171 (January) (2020), 115015, https://doi.org/10.1016/j.applthermaleng.2020.115015.

[21] P. Goli, S. Legedza, A. Dhar, R. Salgado, J. Renteria, A.A. Balandin, Graphene-enhanced hybrid phase change materials for thermal management of Li-ion

batteries, J. Power Sources 248 (2014) 37–43, https://doi.org/10.1016/j.jpowsour.2013.08.135.
[22] K. Zhang, B. Han, X. Yu, Electrically conductive carbon nanofiber/paraffin wax composites for electric thermal storage, Energy Convers. Manag. 64 (2012) 62–67, https://doi.org/10.1016/j.enconman.2012.06.021.
[23] P. Zhang, Z. Meng, H. Zhu, Y. Wang, S. Peng, Experimental and numerical study of heat transfer characteristics of a paraffin/metal foam composite PCM, Energy Procedia 75 (2015) 3091–3097, https://doi.org/10.1016/j.egypro.2015.07.637.
[24] Y. Sheikh, M.F. Orhan, M. Umair, E. Mehaisi, A. Azmeer, Variation in cooling performance of a bio-based phase change material by adding graphene nanoplatelets with surfactants, Int. J. Thermofluids 16 (2022), 100201, https://doi.org/10.1016/j.ijft.2022.100201.
[25] T. ur Rehman, H.M. Ali, A. Saieed, W. Pao, M. Ali, Copper foam/PCMs based heat sinks: an experimental study for electronic cooling systems, Int. J. Heat Mass Transf. 127 (2018) 381–393, https://doi.org/10.1016/j.ijheatmasstransfer.2018.07.120.
[26] A. Alrashdan, A.T. Mayyas, S. Al-Hallaj, Thermo-mechanical behaviors of the expanded graphite-phase change material matrix used for thermal management of Li-ion battery packs, J. Mater. Process. Technol. 210 (1) (2010) 174–179, https://doi.org/10.1016/j.jmatprotec.2009.07.011.
[27] Z. Qu, W.Q. Li, W.-Q. Tao, Numerical model of the passive thermal management system for high-power lithium ion battery by using porous metal foam saturated with phase change material, Int. J. Hydrogen Energy 39 (2014) 3904–3913, https://doi.org/10.1016/j.ijhydene.2013.12.136.
[28] Y. Sheikh, M.F. Orhan, A. Azmeer, Melting performance of a composite bio-based phase change material: an experimental evaluation of copper foam pore size, Int. J. Thermofluids 16 (2022), 100216, https://doi.org/10.1016/j.ijft.2022.100216.
[29] X. Xiao, P. Zhang, M. Li, Effective thermal conductivity of open-cell metal foams impregnated with pure paraffin for latent heat storage, Int. J. Therm. Sci. 81 (1) (2014) 94–105, https://doi.org/10.1016/j.ijthermalsci.2014.03.006.
[30] Y. Zhao, et al., Performance of a liquid cooling-based battery thermal management system with a composite phase change material, Int. J. Energy Res. 44 (6) (2020) 4727–4742, https://doi.org/10.1002/er.5254.
[31] Y. Zhao, B. Zou, J. Ding, Y. Ding, Experimental and numerical investigation of a hybrid battery thermal management system based on copper foam-paraffin composite phase change material and liquid cooling, Appl. Therm. Eng. 218 (2023), 119312, https://doi.org/10.1016/j.applthermaleng.2022.119312.
[32] S.S. Sundarram, W. Li, The effect of pore size and porosity on thermal management performance of phase change material in filtrated microcellular metal foams, Appl. Therm. Eng. 64 (1–2) (2014) 147–154, https://doi.org/10.1016/j.applthermaleng.2013.11.072.
[33] C. Liu, et al., Phase change materials application in battery thermal management system: a review, Materials (Basel) 13 (20) (2020) 1–37, https://doi.org/10.3390/ma13204622.
[34] Y. Li, T. Wang, X. Li, G. Zhang, K. Chen, W. Yang, Experimental investigation on thermal management system with flame retardant flexible phase change material for retired battery module, Appl. Energy 327 (2022), 120109, https://doi.org/10.1016/j.apenergy.2022.120109.
[35] J. Weng, et al., Mitigation effects on thermal runaway propagation of structure-enhanced phase change material modules with flame retardant additives, Energy 239 (2022), 122087, https://doi.org/10.1016/j.energy.2021.122087.
[36] W. Wu, et al., An experimental study of thermal management system using copper mesh-enhanced composite phase change materials for power battery pack, Energy 113 (2016) 909–916, https://doi.org/10.1016/j.energy.2016.07.119.
[37] H. Wang, et al., Heat generation measurement and thermal management with phase change material based on heat flux for high specific energy power battery, Appl. Therm. Eng. 194 (2021), 117053, https://doi.org/10.1016/j.applthermaleng.2021.117053.
[38] A. Tomaszewska, et al., Lithium-ion battery fast charging: a review, eTransportation 1 (2019), 100011, https://doi.org/10.1016/j.etran.2019.100011.
[39] X.-.G. Yang, G. Zhang, S. Ge, C.-.Y. Wang, Fast charging of lithium-ion batteries at all temperatures, Proc. Natl. Acad. Sci. 115 (28) (2018) 7266–7271, https://doi.org/10.1073/pnas.1807115115.
[40] T. Volck, et al., Method for determination of the internal short resistance and heat evolution at different mechanical loads of a lithium ion battery cell based on dummy pouch cells, Batteries 2 (2) (2016), https://doi.org/10.3390/batteries2020008.
[41] Y. Zhu, Y. Fang, L. Su, Y. Fei, Experimental study on thermal performance of a pumped two-phase battery thermal management system, Int. J. Energy Res. 44 (6) (2020) 4664–4676, https://doi.org/10.1002/er.5247.
[42] H. Wang, W. Xu, L. Ma, Actively controlled thermal management of prismatic Li-ion cells under elevated temperatures, Int. J. Heat Mass Transf. 102 (2016) 315–322, https://doi.org/10.1016/j.ijheatmasstransfer.2016.06.033.
[43] L.H. Saw, et al., Novel thermal management system using mist cooling for lithium-ion battery packs, Appl. Energy 223 (December 2017) (2018) 146–158, https://doi.org/10.1016/j.apenergy.2018.04.042.
[44] A.V. Shelke, et al., Characterizing and predicting 21700 NMC lithium-ion battery thermal runaway induced by nail penetration, Appl. Therm. Eng. 209 (2022), 118278, https://doi.org/10.1016/j.applthermaleng.2022.118278.
[45] M. Steinhardt, et al., Low-effort determination of heat capacity and thermal conductivity for cylindrical 18650 and 21700 lithium-ion cells, J. Energy Storage 42 (2021), 103065, https://doi.org/10.1016/j.est.2021.103065.
[46] H. Liu, S. Ahmad, Y. Shi, J. Zhao, A parametric study of a hybrid battery thermal management system that couples PCM/copper foam composite with helical liquid channel cooling, Energy 231 (2021), 120869, https://doi.org/10.1016/j.energy.2021.120869.
[47] PCM-Products, "PlusICE ® Range," vol. 44, no. 0, 2021, [Online]. Available: https://www.pcmproducts.net/files/PlusICERange2021-1.pdf.
[48] J. Zhang, L. Zhang, F. Sun, Z. Wang, An overview on thermal safety issues of lithium-ion batteries for electric vehicle application, IEEE Access 6 (2018) 23848–23863, https://doi.org/10.1109/ACCESS.2018.2824838.
[49] Y. Azizi, S.M. Sadrameli, Thermal management of a LiFePO4 battery pack at high temperature environment using a composite of phase change materials and aluminum wire mesh plates, Energy Convers. Manag. 128 (2016) 294–302, https://doi.org/10.1016/j.enconman.2016.09.081.
[50] A. Hussain, C.Y. Tso, C.Y.H. Chao, Experimental investigation of a passive thermal management system for high-powered lithium ion batteries using nickel foam-paraffin composite, Energy 115 (2016) 209–218, https://doi.org/10.1016/j.energy.2016.09.008.
[51] M. Pan, W. Lai, Cutting copper fiber/paraffin composite phase change material discharging experimental study based on heat dissipation capability of Li-ion battery, Renew. Energy 114 (2017) 408–422, https://doi.org/10.1016/j.renene.2017.07.004.
[52] X. Luo, et al., Experimental investigation on a novel phase change material composites coupled with graphite film used for thermal management of lithium-ion batteries, Renew. Energy 145 (2020) 2046–2055, https://doi.org/10.1016/j.renene.2019.07.112.
[53] R.S. Longchamps, X.-.G. Yang, C.-.Y. Wang, Fundamental insights into battery thermal management and safety, ACS Energy Lett 7 (3) (Mar. 2022) 1103–1111, https://doi.org/10.1021/acsenergylett.2c00077.
[54] J. Wang, et al., Degradation of lithium ion batteries employing graphite negatives and nickel-cobalt-manganese oxide + spinel manganese oxide positives: part 1, aging mechanisms and life estimation, J. Power Sources 269 (2014) 937–948.
[55] G.M. Cavalheiro, T. Iriyama, G.J. Nelson, S. Huang, G. Zhang, Effects of nonuniform temperature distribution on degradation of lithium-ion batteries, J. Electrochem. Energy Convers. Storage 17 (2) (2019), https://doi.org/10.1115/1.4045205.